이학박사 학위논문

# 신경치료 및 분광학적 분석을 위해 특별히 고안된 전기화학 마이크로 프로브

Specific Designed Electrochemical Microprobes for Neural Therapy and Spectroscopic Analysis

2016년 8월

서울대학교 대학원

화학부 전기화학 전공

김 범 진

**A Ph. D. Dissertation**

# Specific Designed Electrochemical Microprobes for Neural Therapy and Spectroscopic Analysis

By

Beom Jin Kim

Supervisor: Professor Taek Dong Chung

Major: Electrochemistry

Department of Chemistry

Graduate School of

Seoul National University

August 2016

## Abstract

# Specific Designed Electrochemical Microprobes for Neural Therapy and Spectroscopic Analysis

**Beom Jin Kim**

**Department of Chemistry, Electrochemistry**

**The Graduate School**

**Seoul National University**

Electrochemistry is an effective analytical method for biological and surface analysis because of monitoring substances without destruction. For this, various-sized probes are used and micro-sized probe is especially useful for practical purposes due to producing optimal spatial resolution.

In Part 1, we introduce a outline of analytical methods and explain why micro-sized electrochemical probe is needed for biological and surface analysis.

In Part 2, Nanoporous Pt with extremely small (1–2 nm) and uniform nanopores, $L_2$-ePt, was electrochemically investigated in embryo brain. For comparison study

under precise control of electrochemical potential, we constituted an electrochemical cell beneath the embryo surface by introducing a flat and a nanoporous Pt twisted wires around which a Ag/AgCl wound. $L_2$-ePt and flat Pt in the brain were compared with each other by conventional voltammetry and electrochemical impedance spectroscopy at the dc bias, which was carefully selected to minimize faradaic interference. The electrochemical behavior at $L_2$-ePt implanted in embryo brain is immune to severe passivation and closer to an ideal capacitor than flat Pt. Lower electrode impedance of $L_2$-ePt leads to less potential drop at the interface between the electrode and the extracellular solution, protecting the implanted system from unwanted faradaic reactions. Various aspects including the low electrode impedance and electrochemical stability of $L_2$-ePt in the embryo brain suggest $L_2$-ePt as a promising electrode material for effectively stimulating distant neuronal cells and recording local field potential signals.

In Part 3, we suggest a new strategy for probe fabrication to simultaneously acquire electrochemical signals from ultramicroelectrode (UME) and spectroscopic information from surface-enhanced Raman scattering (SERS). The proposed Electrochemical-SERS (EC-SERS) probe was prepared by elaborately tuning the SERS-active gold microshell (μ-shell) to maximize Raman scattering, mechanically fixing it at the end of micropipette, and electrically connecting with the ruthenium inner layer through electroless deposition process. This μ-shell based SERS-active UME is barely smaller than the laser focal volume (ca. 2 μm in diameter) but still visible through optical microscope. It proposes novel

opportunities to scanning electrochemical microscope (SECM) that enables gap-mode free in situ EC-SERS analysis in electrochemical and biological systems.

***Keywords***: Nanoporous electrode, neural recording and stimulation, Microporobe, Electrochemistry, Gold microshell, Raman spectroscopy, Ultramicroelectrode

***Student number***: 2007-22817

# Contents

## PART 3. Specific Designed EC-microprobe for EC reaction

# List of Figures

voltammograms at 50 mV $s^{-1}$ in 0.5 M $H_2SO_4$ before (dashed line) and after (solid line) $L_2$-ePt electrodeposition.

**Figure 2-4.** The placement of three electrodes in embryo's brain.

**Figure 2-5.** TEM images of the L2-ePt. Both images were reproduced with permission from [31].

**Figure 2-6.** Evaluation of insulation by the cyclic voltammograms at 50 mV $s^{-1}$ in 0.5 M $H_2SO_4$ solution (solid line) and a deeper place (dashed line) in the same solution.

**Figure 2-7.** Cyclic voltammogram of $L_2$-ePt in the buffer solution.

**Figure 2-8.** Cyclic voltammograms of (a) the flat Pt and (b) $L_2$-ePt inserted in the brain at10 mV $s^{-1}$. Twisted RE denotes the Ag/AgCl wire, which is wound around the WEs.

**Figure 2-9.** (a) Bode plots in the frequency range of 1 Hz-100 kHz at the flat Pt (circle) and $L_2$-ePt (triangle) in the buffer solution (open) and in the brain (filled). (b) Impedance data for bulk solution and the electrode and (c) the ratio of bulk solution (gray) and electrode impedance (dark).

**Figure 2-10.** (a) Nyquist plots theoretically predicted from the dummy circuit consisting of a resistor and a capacitor in series and (b) Nyquist plots from the experiments in the buffer solution and the brain under non-faradaic conditions. In (b), the data from flat Pt (circle) and $L_2$-ePt (triangle) were fitted using the equivalent circuit with constant phase element based on transmission line model

(TLM). The curves fitted to the data from flat Pt are dashed lines and those from $L_2$-ePt are solid lines, respectively. Insets show the magnified view in the high frequency domain. The dc offset potential is +0.2 V and the amplitude of alternating current potential is 10 mV. (c) Adopting the TLM for fitting (left), we calculated α values in the brain (in table on the right).

**Figure 2-11.** Bode plots from flat Pt (circle) and $L_2$-ePt (triangle) in (a) buffer solution and (b) brain. The $|Z|$ of a y-axis in the Bode plots indicates $Z_{Re}$ (closed) and $Z_{Im}$ (open) values $Z_{RE}$ (closed), $Z_{Im}$ (open). The $Z_{Re}$ values in the Bode plots were corrected with the solution resistances. The data were fitted based on an equivalent circuit for TLM presented in Figure 2-10(c). The curves fitted to the data from flat Pt are dashed lines and those from $L_2$-ePt are solid lines.

**Figure 2-12.** Nyquist plots in the buffer solution before (closed triangle) and after (opened triangle) implantation and in the brain (closed circle).

**Figure 2-13.** Nyquist plots in the buffer solution (opened circle) and bovin serum albumin in the buffer solution (closed circle).

**Figure 2-1.** FE-SEM image of a EC-SERS gold μ-shell which has been plated 20 times. The scale bar in the lower right denotes 0.5 μm.

**Figure 3-2.** Schematic illustrations of the process to exchange solutions. (a) Adding the excess water to the micropipette with the gold μ-shell in the gold μ-shells/$KAuCl_4$ solution. (b) Removing the diluted $KAuCl_4$ solution. (c) For

electroless plating process, add the reducing solution to the micropipette with the gold μ-shell in water.

**Figure 3-3.** (a) Schematic and (b) Optical microscope images of a gold μ-shell to the end of a micropipette according to the electroless deposition procedure. The scale bars denote 5 μm.

**Figure 3-4.** (a) A SERS spectrum of Py adsorbed on the EC-SERS probe in 0.1 M Py solution in 0.1 M $NaClO_4$ at -0.6 V applied potential. (b) The detailed peak assignment of (a) which agrees exactly with reported previously SERS spectra.[10,38]

**Figure 3-5.** Schematic illustration of the proposed electrochemical SERS monitoring system based on a well-defined EC-SERS probe. A gold μ-shell *ca.* 2 μm in diameter at the end of the probe acts as a sensitive SERS substrate and a UME with well-defined geometry and dimensions. The μ-shell perfectly fits the focal volume of the laser beam used in this work, a He/Ne laser (632.8 nm, 3 mW).

**Figure 3-6.** Fabrication of the EC-SERS probe. A SERS-active gold μ-shell was simply attached to the end of a micropipette by suction with negative pressure (a–b), and electrically connected with a conductive inner layer by heterogeneous electroless deposition (c).

**Figure 3-7.** Construction and evaluation of the EC-SERS probe. (a) Optical and (b) FE-SEM image of the probe. Horizontal scale bar represents 2 μm. (c) Steady state voltammogram in 5 mM hexaammineruthenium (III) chloride aqueous solution

containing 0.1 M KCl as the supporting electrolyte (scan rate, 0.03 V $s^{-1}$). (d) SERS spectrum from the probe modified by 4-nitrobenzenethiol.

**Figure 3-8.** (a) The schematic view of the electrochemical reduction of the NBT on the probe, (b) a chemical equation of the reduction of nitrobenzene to aniline through three 2-electron steps, (c) potential dependent SERS spectrum in 0.1 M $H_2SO_4$.

**Figure 3-9.** (a) The schematic view of the electrochemical reduction of the NBT on the probe, (b) a chemical equation of the reduction of nitrobenzene to aniline through three 2-electron steps, (c) potential dependent SERS spectrum in 0.1 M $H_2SO_4$.

**Figure 3-10.** (a) SERS spectra of pyridine adsorbed on the gold μ-shell probe acquired at a variety of electrode potentials. Probe potential was swept from 0.4 V (bottom) to –0.8 V and back to 0.4 V (top) at 0.02 V $s^{-1}$. (b) Dependence of the relative intensity of two bands, (1) *ca.* 1008 $cm^{-1}$ and (2) *ca.* 1029 $cm^{-1}$. The SERS intensity normalized by the aqueous perchlorate stretch band (*ca.* 930 $cm^{-1}$), which corresponds to the peak marked with an asterisk in Figure 3-4(a). All spectra were taken using a 632.8 nm line from a 3 mW He–Ne laser with an integration time of 10 s.

# PART 1.

## General Introduction

# 1. Introduction

Analytical chemistry is the branch of chemistry that deals with determining the identity and concentration of chemical substances. For analysis of the biomolecules and chemical species at the special region, a selective detection among mixtures of compounds become more important. A number of methods are used in classical analysis to perform these tasks (Figure 1-1). Qualitative as well as quantitative analysis of mixtures can be achieved by chromatographic methods such as gas chromatography (GC) and liquid chromatography (LC).[1] Identification of pure compounds can be achieved by mass spectrometry (MS). Chemical or biological sensors and fluorescence spectroscopy can also be employed for selectively quantifying a compound in a mixture. Electron microscope (EM) give structural information even in the presynaptic terminals between neurons and neurotransmitter release.[2] The atomic structure of potassium selective ion channels has been solved by x-ray crystallography.[3]

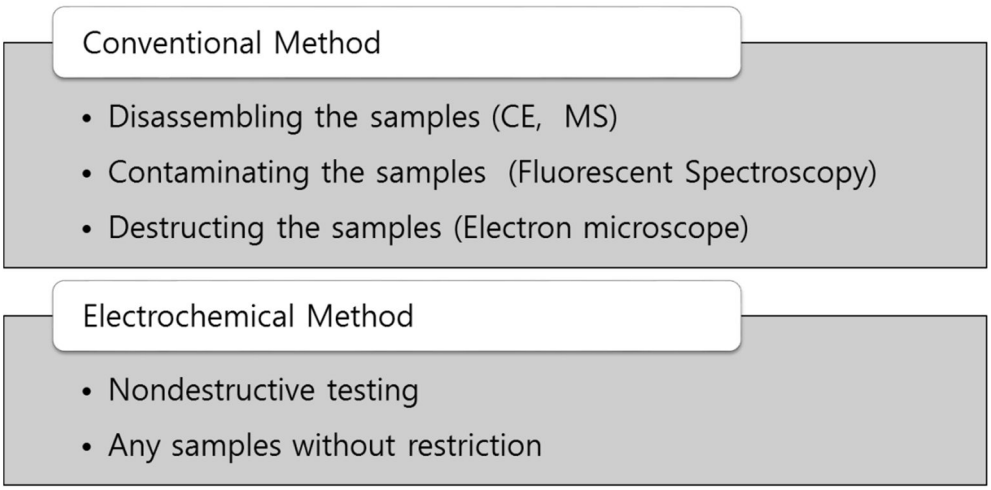


**Figure 1-1.** Advantages and disadvantages of conventional analytical methods and the strengths of electrochemical method.

But most of these classical methods are not suitable for bioanalysis and surface analysis because these analysis need a nondestructive method without deformation of substances. The sampling procedures are necessary for CE and MS. Fluorescent spectroscopy contaminates the samples by adding a fluorescent tag. EM also destroy the samples by applying strong electron energy. On the other hand, an electrochemisty is an appropriate method for the nondestuctive analysis because any substances can be examined by putting the electrochemical analysor.[4] Furthermore, it provides the information of dynamics of substances through the real time monitoring.

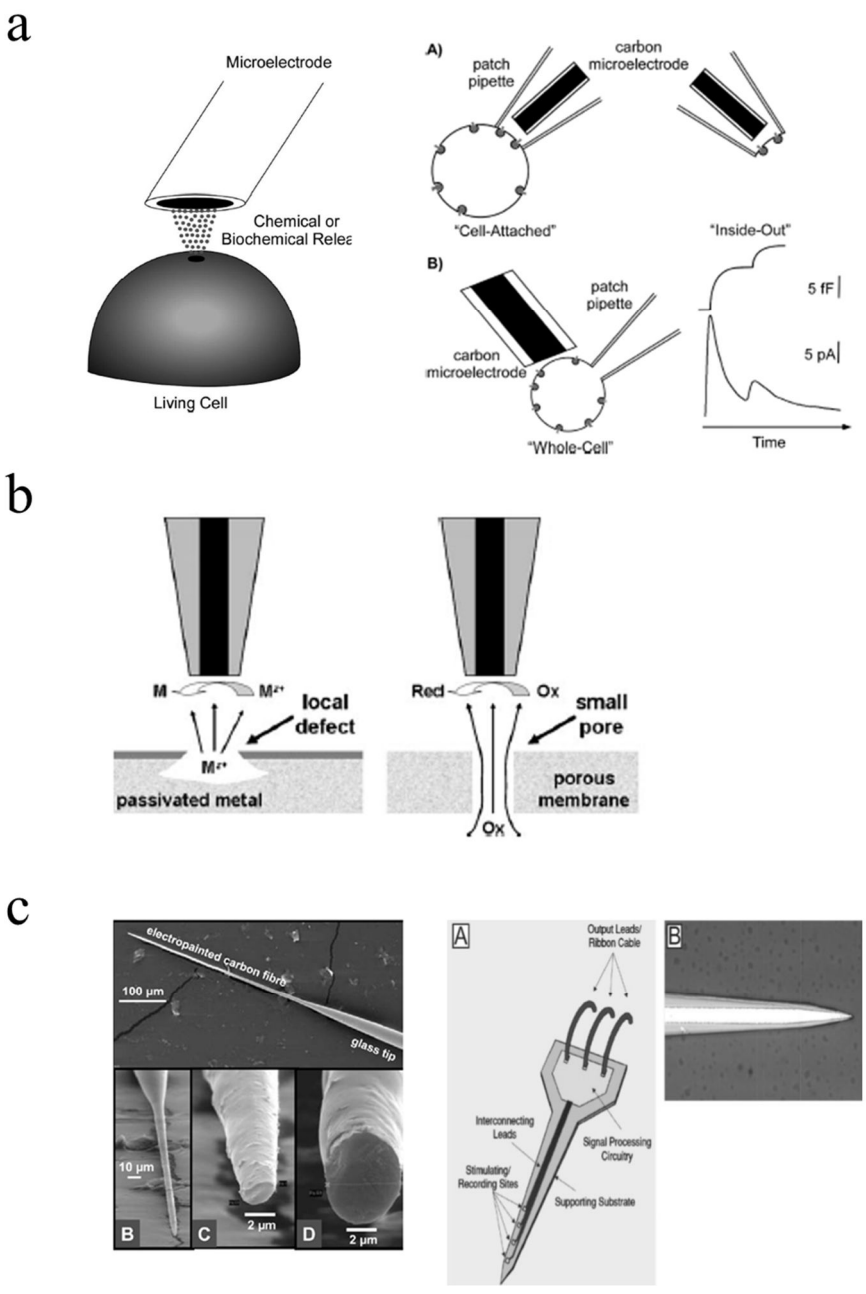


**Figure 1-2.** An electroactive species produced at small active sites on (a) biological

(adapted from reference 5) and (b) metal and membrane surfaces (adapted from reference 4). (c) Small-sized electrochemical probes (adapted from reference 6, 7).

An electroactive species at small active sites can be detected by electrochemical method as well. Figure 1-2(a) shows the release of chemical messenger molecules at the restricting the volume of the single cell.[5] Figure 1-2(b) shows the release of chemicals from tiny pores by locally corroding and semipermeable membranes.[4] In these cases, the electrochemical probes have to be smaller and various probes were developed for these purposes in Figure 1-2(c).[6,7] Therefore, selecting the size of probes adequate to an object of investigation become important.

With regard to biological study, especially neural recording and stimulation, nano-sized probes are used for specific examination at the single cell level.[8,9] But the nanoprobe restricts the research field within academic area because it is not suitable for the most applications implanted in the tissue. The nanoprobe is also used in the surface analysis, particularly on an electrochemical reaction such as a surface confined reaction and a electrochemical reaction within an electric double layer.[10] But it is also not suitable for practical uses due to limited studies on the flat surface and the hard positions of the probe. Meanwhile micro-sized probe is increasingly important in many practical approaches interested in the reactions in a diffuse layer within several tens micrometers. Moreover, most studies using nanoprobes have trouble to precise measurements due to less mechanical stability and large electrode impedance of the probe and an indefinable actual shapes of the

probe.[11] After all, micro-sized probes is proper to be used in these researches.

In this doctoral dissertation, we specially designed micro-sized electrochemical probes and verified their properties. This probe enables a close examination implanted in brain even in nanoporous electrode. Also, we proposed a creative probe with a simultaneous spectroscopic analysis for confirmation of chemical identity in electrochemical reactions.

# 2. References


(1) Mans, A.; Pamme, N.; lossfidis D. *Bioanalytical Chemistry*; Imperial College Press (ICP), First published 2004, Peprinted 2008

(2) Heuser, J. E.; Reese, T. S.; Dennis, M. J.; Jan, Y.; Jan, L.; Evans, L. *The Journal of cell biology* **1979**, 81, 275-300

(3) Doyle, D. A.; Cabral, J. M.; Pfuetzner, R. A.; Kuo, A.; Gulbis, J. M.; Cohen, S. L.; Chait, B. T.; MacKinnon, R. *Science* **1998**, 280, 5360

(4) Schulte, A.; Schuhman, W. *Angew. Chem. Int. Ed.* **2007**, 46, 8760-8777

(5) Amatore, C.; Arbault, S.; Guille, M.; Lemaıˆtre, F. *Chem. Rev.* **2008**, 108, 2585-2621.

(6) Bauermann, L. P.; Schuhmann, W.; Schulte, A. *Phys . Chem. Chem.* **2004**, 6, 4003-4008

(7) Wise, K. D. *IEEE Eng. Med. Biol. Magazine* **2005**, 24, 22.

(8) Beaulieu, I.; Kuss, S.; Mauzeroll, J. *Anal. Chem.* **2011**, 83, 1485-1492;

(9) Amemiya, S.; Guo, J.; Xiong, H.; Gross, D. A. *Anal. Bioanal. Chem.* **2006**, 386, 458-471

(10) Sonnenfeld, R.; Hansma, P. *Science* **1986**, 232-211

(11) Arrigan, D. W. M. *Analyst* **2004**, 129, 1157

# PART 2.

## Specific Designed EC-microprobe for Neural Recording and Stimulation

# 1. Introduction

The attention to electrical neuromodulation is continuously rising with recent advances in neuroscience and prosthetic engineering. Clinical therapy using small electrodes has emerged to be one of the attractive fields in the treatment of various disorders such as pain management, hearing augment, and movement disorders.[1-2] Accordingly, understanding what happens at the electrode implanted in human body is required for developments in new electrode materials that ensure higher efficiency and safety.

The electric signal in a neuron is transmitted in the form of action potential (AP).[3] Quick opening and closing of the ion channels generate a ion distribution disparity across the membrane, leading to an electrical potential difference. Such potential difference known as the transmembrane potential causes AP propagation along the neuron.[3] For the study of neural networks, the AP should be recorded. To do so, the potential difference produced by the ion distribution needs to be converted to the electric signal with minimal signal diminishment as well as low noise. That is why close proximity of the electrode to the neuron is crucial. We can express such a system as a circuit composed of two separate domains, i.e. electronics and biochemical electrolyte, in which electrons and ions act as charge carriers, respectively. Those two different worlds border on each other at the electrode interface where they are electrically connected through non-faradaic process, possibly accompanied by faradaic reaction.[4] This makes both the neural

recording and stimulation complicated. Sometimes we have to analyze the experimental results in view of electrochemistry. Electroanalytical approach provides valuable knowledge to understand what have caused the electric responses from the electrode near a neuron. Electrochemical methods are useful to detect biological properties in real time because they are less destructive and very rapid compared to fluorescence-based imaging, requiring no chemical additive.

A number of microelectrodes has been introduced for in vitro or in vivo applications[5-11] ever since electric signals from cultured cells were recorded by the microelectrode array 40 years ago.[12-13] Surface area of microelectrodes is normally less than 0.01 $mm^2$ because small electrode area should be advantageous for stimulating the specific tissue near which it is implanted and also recording neural signals with high spatial resolution.[4]

However, smaller geometric surface area of the microelectrodes results in higher electrode impedance ($Z_e$), which is problematic for the purpose of neural recording as well as stimulating. Potential drop is proportionally concentrated at the interface between the electrode surface and the tissue to which the electrode is exposed. As a result, less portion of the overall potential applied ($E_{appl}$) is exerted on the targeted tissue distant from the working electrode (WE).[14-15] Therefore, we must apply higher $E_{appl}$ to stimulate the tissue as effectively as when using larger electrodes. This is likely to lead to faradaic reaction, possibly producing toxic chemicals. In neural recording, small electrode is unfavorable in detecting electric neural signals such as local field potential (LFP) at the expense of spatial resolution.

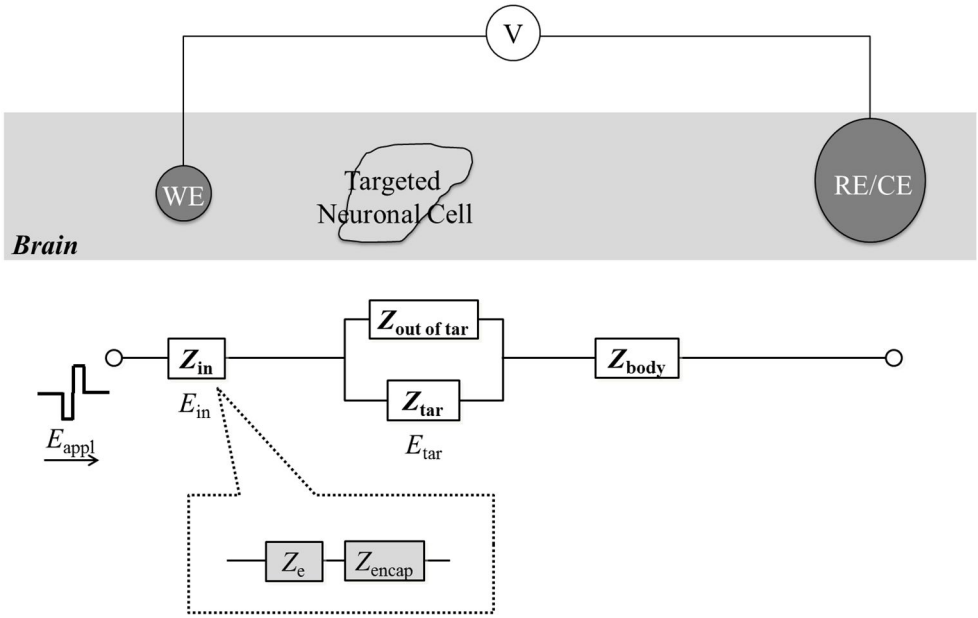


**Figure 2-1.** The schematic view of equivalent circuit illustrating potential drop distribution along the impedance components for conventional neural stimulation using two electrodes when an external potential bias, $E_{appl}$, is applied to stimulate a targeted neuronal cell in the brain. The total impedance consists of the electrode-tissue interface ($Z_{in}$), the targeted neuronal cell ($Z_{tar}$), the neurons or tissues out of the target ($Z_{out\ of\ tar}$), and distant body ($Z_{body}$). $Z_{in}$ consists of $Z_e$ and impedance of encapsulation ($Z_{encap}$), which results from immune reaction upon foreign body, i.e. electrode. The potential drops at the electrode-tissue interface ($E_{in}$) and the targeted neuronal cell ($E_{tar}$) are parts of $E_{appl}$, which are proportional to $Z_{in}$ and $Z_{tar}$, respectively.

Figure 2-1 explains how potential drop should be distributed along the circuit components if two electrodes are implanted at regions significantly apart from each other. A targeted neuronal cell between WE and RE/CE should be taken into account as a part causing the potential drop proportional to the respective impedances: the electrode-tissue interface ($Z_{in}$), the targeted neuronal cell ($Z_{tar}$), the neurons or tissues out of the target ($Z_{out\ of\ tar}$), and the rest of body distant from the WE ($Z_{body}$) as shown in Figure 2-1. Because the potential drop of targeted neuronal cell ($E_{tar}$) is the proportional to $Z_{tar}$ to the total impedance ($Z_{tot}$) according to Kirchhoff's law, $E_{tar} \propto Z_{tar}/Z_{tot}$, so that larger $Z_{in}$ including $Z_e$ should lead to greater potential drop at the electrode-tissue interface. Since the potential drop close to $E_{appl}$ at the targeted cell is required to effectively exert electric stimulation on the target and also to measure neural signals from the target, it is desirable to make $Z_{in}$ as low as possible.[16-17]

$Z_{in}$ changes as a function of the time elapsed after implantation,[18-20] due to foreign body reactions such as long-term inflammation and glial scar formation between the electrode and the tissue.[21] This makes it difficult to predict how the neural response and stimulation condition would vary once electrodes are implanted for prolonged experiments or therapy. Furthermore, $E_{appl}$, which is needed to stimulate the region of our interest, keeps increase because the insulating tissues grow surrounding the electrode surface, leading to increasing $Z_{encap}$. As a consequence, larger portion of potential drop takes place at the electrode-tissue

interface rather than the targeted zone that is away from the electrode. Higher $E_{appl}$ to compensate the drop at the electrode may bring about side reactions. Moreover, it is not easy to assess the chronic $Z_{in}$ change, resulting in practical difficulty in stimulating reproducibly and safely under the condition that varies with elapsed time and patient-by-patient.[22-24]

To resolve this challenge, a few potential solutions can be proposed, one of which is modifying the electrode surface with biocompatible materials to mitigate immune reactions, as found in implantable sensor researches.[25-28] Another way is to reduce $Z_{in}$ as much as possible. Minimal $Z_{in}$ allows low $E_{appl}$ while ensuring a sufficient potential drop at the targeted neuronal cell, in spite of inevitable immune reactions. Low $E_{appl}$ at the electrode offers an additional benefit, suppressing the probability of faradaic reaction that may produce unwanted chemical species.

$Z_{in}$ of the implanted electrode consists of $Z_e$ and $Z_{encap}$, where the increase of $Z_{encap}$ is unavoidable. Therefore, $Z_e$ must be kept as low as possible in order to make the influence of $Z_{encap}$ negligible compared to $Z_{tar}$. To do so, nanoporous electrode is a promising answer because it provides a much larger real surface area compared to a flat electrode with the same apparent area. In this regard, various porous materials have been reported to not only lower the electrode impedance but also raise the charge injection capacity for better recording and stimulation.[4,29]

In particular, $L_2$-ePt shows extremely low electrode impedance and correspondingly large charge injection capacity.[30] It has minuscule pores of 1–2 nm in diameter, which are comparable to the thickness of electric double layer, indeed

one of the smallest size as far as the electrode works.[31] In addition to the maximal surface enlargement, three-dimensional network of $L_2$-ePt leads to higher electrokinetic activity.[32] Also, its uniform structure and three-dimensional pore inter-connectivity enable fast charging dynamics, resulting in successful conductometric detections in ion chromatography, even without ion suppressor at high ionic strength.[33] Moreover, $L_2$-ePt offers even better mechanical stability than conventional platinized Pt.[30]

The behavior of $L_2$-ePt as an electrode material in vitro was previously reported[30], and other comparable nanoporous electrodes have recently shown to suffer less from noise in neural recording[34]. In spite of its attractive characteristics, the electrochemical performance of $L_2$-ePt has not been investigated when implanted in the brain. Intensive electrochemical analysis is essential to look into how $L_2$-ePt works in animal body. In this work, we implanted a reference electrode (RE) positioned close to two WEs to accurately control the electric potential applied to the system.[35] Both a flat and a $L_2$-ePt as working electrodes were inserted into a single spot of embryo brain for comparison study on the effect of nanoporous material for electrochemistry in the brain. The two WEs were placed as close to each other as possible so that the extracellular environments surrounding those after implantation should be almost the same. For this study, we chose the brain of rat embryo having softer tissues than that of an adult rat. The soft tissue of embryo is appropriate to reduce unexpected mechanical damage of the electrode surface. Electrochemical impedance spectroscopy (EIS) with nanoporous electrode in

embryo brain was performed, and it is believed that the results carry significant implication for the research and engineering of embryonic developments as well.

# 2. Experimental Methods

## 2.1. Reagents

All chemicals including hydrogen hexachloroplatinate hydrate (Kojima chemicals, Japan), *t*-octylphenoxy polyethoxyethanol (Triton X-100, Sigma), sodium chloride (Daejung, Korea), sulfuric acid (Sigma), and Dulbecco's Phosphate Buffered Saline (DPBS, Welgene, LB001-02) were used without further purification. All aqueous solutions in this experiment were prepared with ultrapure deionized water produced by NANO pure (Barnstead). A Pt wire (A-M Systems, #772000, 76 μm), a Ag wire (Sigma Aldrich, 100 μm), and a Pt wire (Sigma Aldrich, 500 μm) were for the working electrode, the reference electrode, and the counter electrode, respectively. Bovine serum albumin (A2153, Sigma) was used for adsorption experiments.

## 2.2. Electrode Preparation and Electrodeposition of $L_2$-ePt

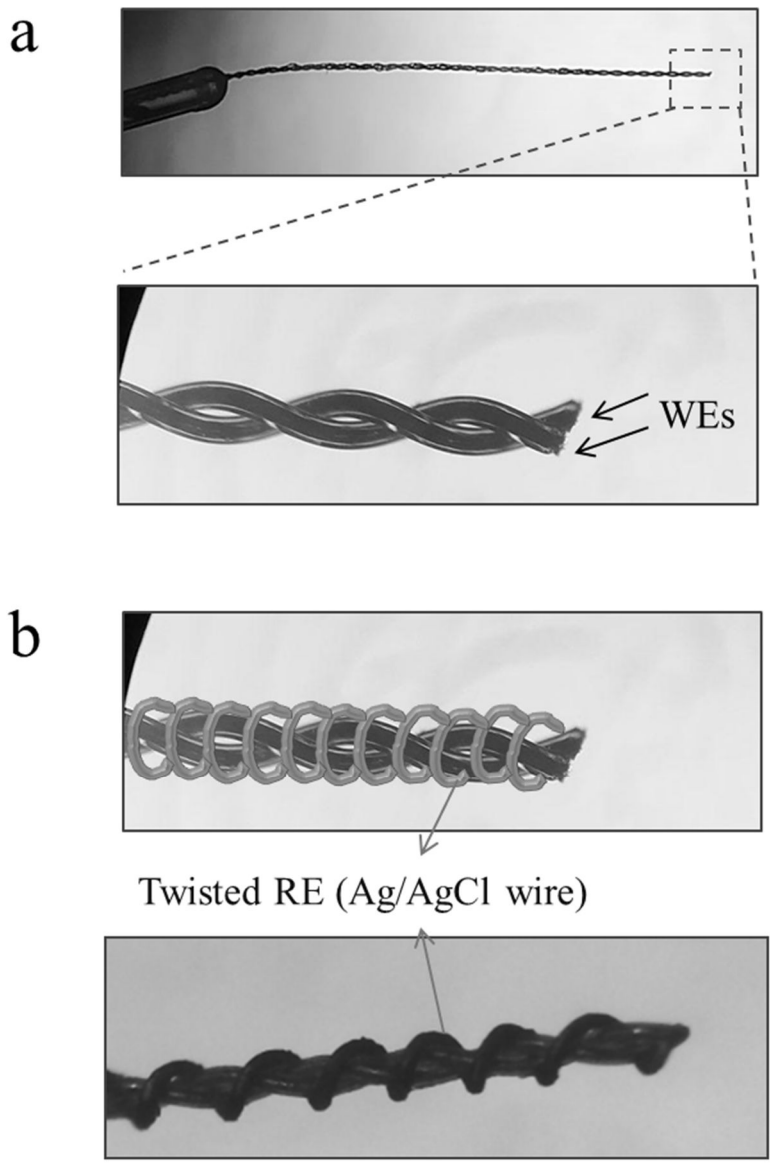


**Figure 2-2.** Preparation of the twisted microelectrodes with RE. (a) Two WEs of flat Pt and $L_2$-ePt are twisted to compare and (b) the RE is a Ag/AgCl wire and coiled around a pair of WEs. The WEs are shrouded with perfluoroalkoxy for

insulation.

To prepare the twisted microelectrodes (Figure 2-2(a)), a Pt wire was bent in half and the two ends were attached to a stirring bar while the loop was suspended on a stand. The wires were twisted as the stirring bar rotated one hundred times in the forward direction and ten times in the reverse direction to relieve the excessive tension. Then, the twisted Pt wire was evenly heated using a heat gun (Bosch, GHG 500-2). Cooling the wire for 30 s was followed by carefully cutting it from the stand. We wound an Ag wire around the twisted Pt wires in the same way (Figure 2-2(b)). The twisted Pt and Ag wires were inserted into a glass tube, and one side of the twisted wires was connected to a conductive electric wire (Smekorea, AWG22, 57.4 ohm/km) for the electric contact.

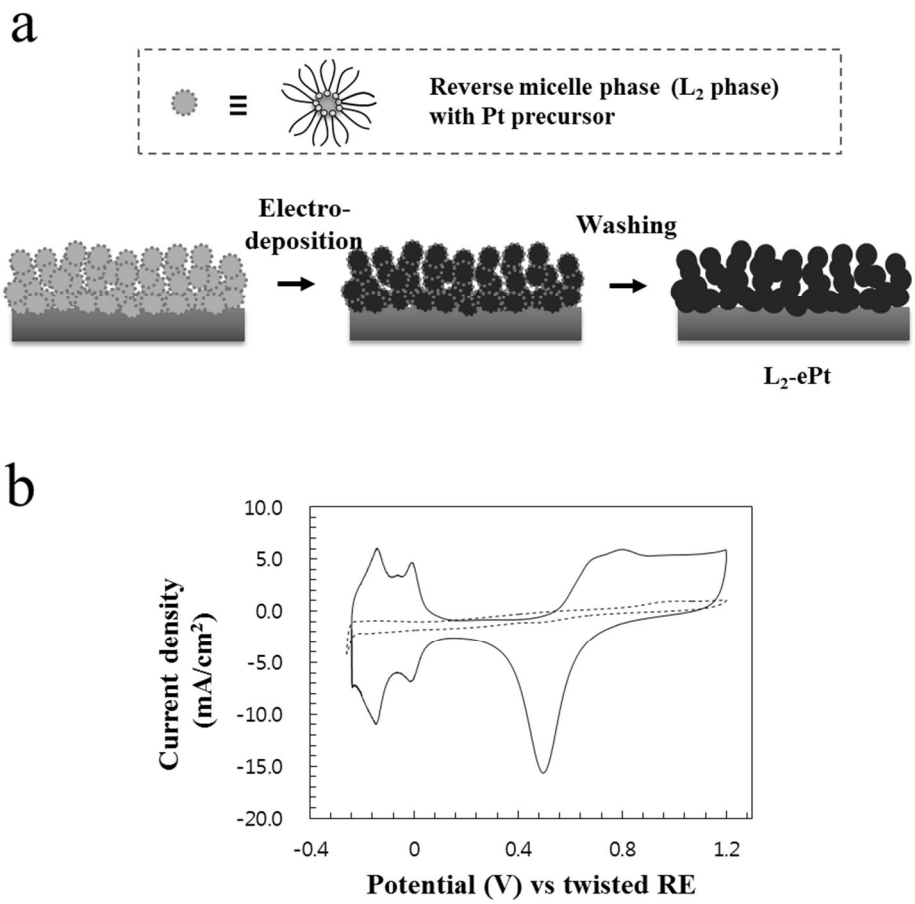


**Figure 2-3.** (a) Electrodeposition process of $L_2$-ePt from a $L_2$ phase. (b) The cyclic voltammograms at 50 mV $s^{-1}$ in 0.5 M $H_2SO_4$ before (dashed line) and after (solid line) $L_2$-ePt electrodeposition.

In Figure 2-3(a), $L_2$-ePt was prepared by electroplating Pt in a reverse micelle solution as described in a previous report.[31] The plating solution of hydrogen

hexachloroplatinate hydrate (5 wt%), 0.3 M sodium chloride (45 wt%), and Triton X-100 (50 wt%) was heated at 60 °C and gently stirred till a homogeneous solution was obtained. Temperature of the plating solution was maintained around 40–43 °C during electroplating using a constant-temperature water bath. We electrodeposited $L_2$-ePt on one of two twisted Pt wires at –0.18 V vs. Ag/AgCl (3 M NaCl, RE-5B, BAS Inc.). Electroplating on the microelectrode required the lower plating potential than that of macroelectrode. To eliminate the Triton X-100 after electroplating, the twisted wire was immersed in warm distilled water (50–60 °C) for 30 min, and this procedure was repeated 3–4 times. Finally, the electrode was electrochemically cleaned by applying a cycling potential between +1.2 and –0.26 V vs. Ag/AgCl (3 M NaCl, RE-5B, BAS Inc.) in 0.5 M $H_2SO_4$ until reproducibly identical cyclic voltammograms were obtained. Electrochemical cleaning without eliminating the Triton X-100 in warm distilled water made large cracks and a lack of reproducibility of the electroplating. The Ag wire was electrolyzed at 0.4 V for 2000 s in 3 M NaCl so that the resulting Ag/AgCl reference electrode was in vicinity to the twisted Pt wires.

## 2.3. Brain of Embryo as an Electrochemical Cell

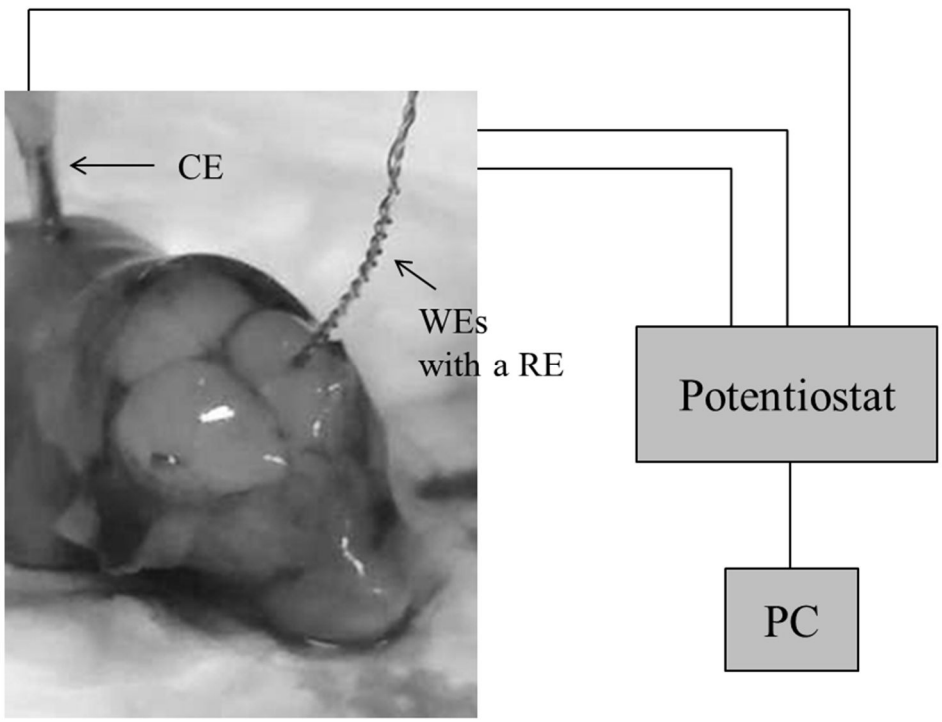


**Figure 2-4.** The placement of three electrodes in embryo's brain.

## 2.4. Electrochemical Measurements

All electrochemical measurements were performed in a three electrode system using Model CHI604B (CH Instruments) as electrochemical analyzer. One of twisted Pt microelectrodes was a bare flat (polycrystalline) Pt while the other was a nanoporous Pt, $L_2$-ePt. For EIS experiments, Model Reference 600 (Gamry Instruments) equipped with EIS300, a software for analysis, was used. A programmed ac input with 10 mV amplitude in the frequency range from 1 Hz to

100 kHz was superimposed on the dc potential where no faradaic reaction occurred. All experiments were carried out at room temperature.

The embryos were taken from Sprague-Dawley rats (Koatech) at day 18 of gestation (E18). The abdomen and uterus of the pregnant rat were dissected during isoflurane anesthesia in rats, and the embryos were collected carefully and immediately placed in Hank's buffered salt solution to maintain the stability of tissue until the next process. Embryo was mounted in a homemade experimental stand and the meninges and the skull were removed by a fine-tipped forceps (Dumont no.5). The twisted Pt and Ag/AgCl wires were inserted into the cerebrum of brain with about 1 mm in depth and the CE was fixed in the back of the embryo. Figure 2-4 shows how the three-electrode system was constituted and where the electrodes were implanted in the embryo brain. To investigate the effect of brain tissue as an electrolyte medium for electrochemistry, we did control experiments in a buffer solution, DPBS. For shielding from environmental electronic noise, all experiments were conducted in a faraday cage (Vistashield Faraday Cage, Gamry Instrument) grounded. All conducting materials within the cage such as metal stand and clip were electrically connected to the faraday cage for protecting the system from noise.

## 2.5. Fitting Procedure of Electrochemical Impedance Spectroscopy

To analysis of electrochemical results from $L_2$-ePt, we adopted the Transmission line model (TLM) which was proposed by de Levie[36] and generally used for modeling porous electrodes in electrochemical impedance spectroscopy.[37,39] The α values were obtained by fitting the experimental data as shown in Figure 2-10(c) using pre-built EIS model (Bisquert Open model, BTO) in Gamry's Echem Analyst software. Although a resistor and a CPE in parallel are in BTO, we considered only CPE element, $q$, neglecting the parallel resistance because the proposed system was carried out under the condition assuming the absence of faradaic reaction. The film thickness was assumed to be 1 μm according to result of the previous report[32].

## 2.6. Interpretation of the Bode plots.

Figure 2-11 shows the Bode plots for flat Pt (circle) and $L_2$-ePt (red triangle) in (a) buffer solution and (b) brain. The $|Z|$ of a y-axis in the Bode plots means $Z_{Re}$ (closed) and $Z_{Im}$ (open) values which were corrected with the solution resistances. The data were fitted based on TLM in Figure 2-10(c) where the curves fitted to the data from flat Pt are dashed lines and those from $L_2$-ePt are solid lines. $L_2$-ePt showed similar behavior to that in the previous report[33], i.e. a plateau in the intermediate frequency region and two parallel lines between log ($Z_{Re}$- $R_s$) and log $Z_{im}$ with a slope of – α in the low frequency region. The slope let the α value of CPE calculated and the α values of $L_2$-ePt are higher than those of flat Pt in the low frequency range in both the buffer solution and the brain. Those results were

consistent with those of Nyquist plot in Figure 2-10, indicating that the characteristic behavior of $L_2$-ePt is closer to pure capacitance.

# 3. Results and Discussion

## 3.1. Voltammogram in the cerebrum

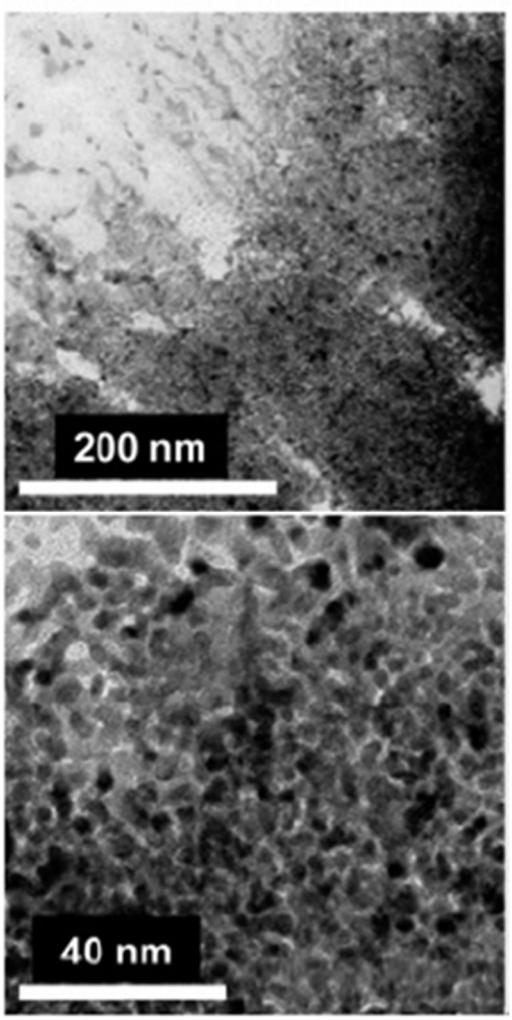

**Figure 2-5.** TEM images of the L2-ePt. Both images were reproduced with permission from [31].

The TEM images of the flat Pt and $L_2$-ePt ensure that the structure of $L_2$-ePt has numerous interconnected pores (Figure 2-5).[31] Figure 2-3(b) shows the cyclic voltammetric responses of the flat Pt and $L_2$-ePt in 0.5 M $H_2SO_4$ at 50 mV $s^{-1}$. While the WEs had the same apparent surface area of the 4.5 $\times$ $10^{-5}$ $cm^2$, much larger current of $L_2$-ePt at the cyclic voltammogram indicates that it has greatly enlarged real surface area compared with the flat Pt. The roughness factor ($f_R$ = real surface area/apparent surface area) of the $L_2$-ePt ($f_R$ 126) was determined by measuring the area under the hydrogen adsorption peak of the cyclic voltammogram using 210 μC $cm^{-2}$ of the conversion factor[38] in Figure 2-3(b).

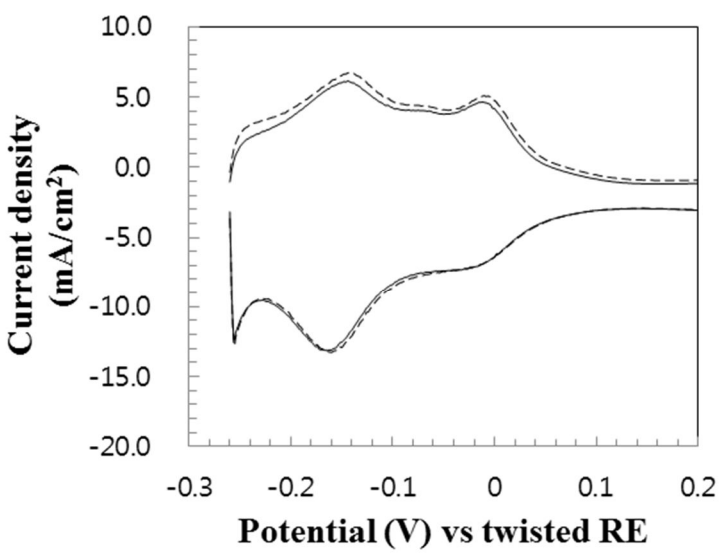

**Figure 2-6.** Evaluation of insulating property of the twisted microelectrodes by the cyclic voltammograms at 50 mV $s^{-1}$ in 0.5 M $H_2SO_4$ solution (solid line) and a deeper place (dashed line) in the same solution.

To evaluate insulating property of the twisted microelectrodes, we compared with the cyclic voltammogram obtained in a deep place of 0.5 M $H_2SO_4$ solution (Figure 2-6). There was no difference and we proved that the twisted microelectrodes has a good insulation.

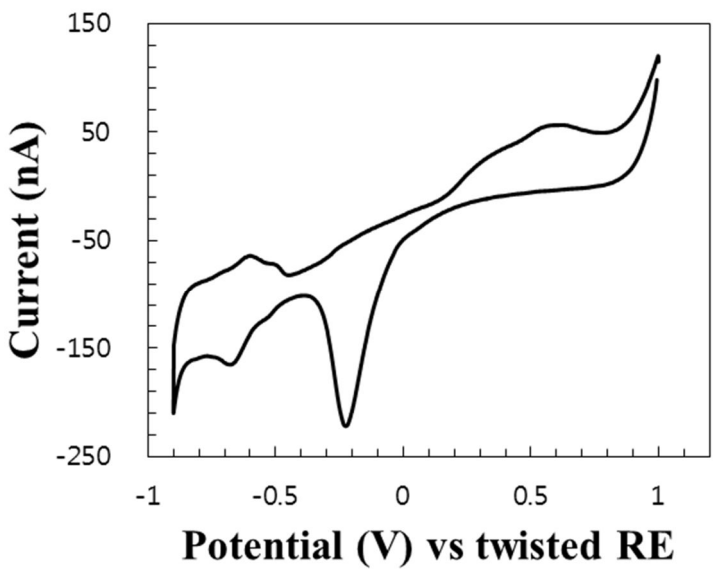


**Figure 2-7.** Cyclic voltammogram of $L_2$-ePt in the buffer solution.

a

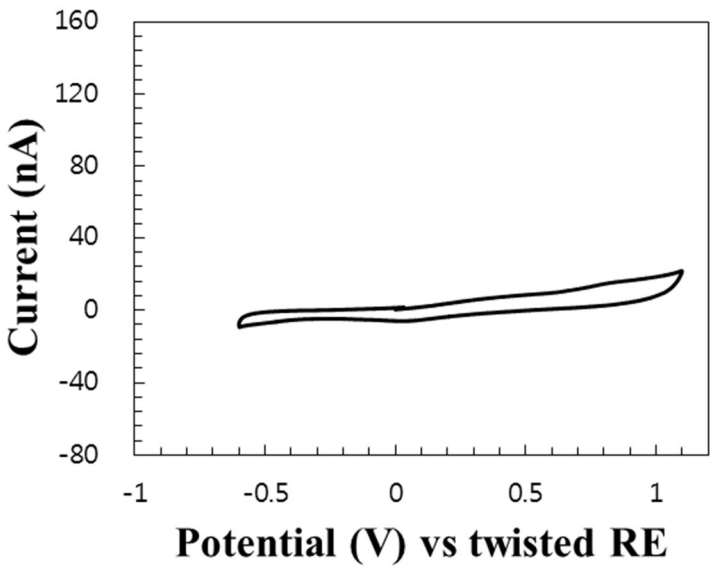
160
120
80
40
0
-40
-80
Current (nA)
-1
-0.5
0
0.5
1
Potential (V) vs twisted RE

b

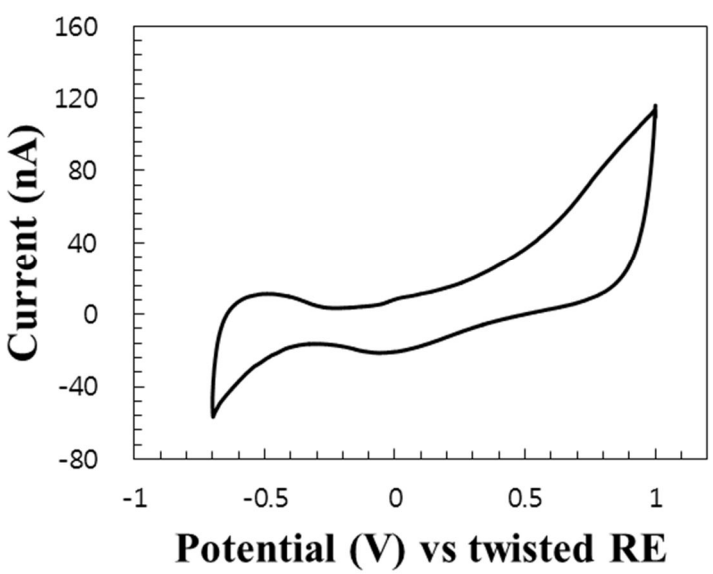
160
120
80
40
0
-40
-80
Current (nA)
-1
-0.5
0
0.5
1
Potential (V) vs twisted RE

**Figure 2-8.** Cyclic voltammograms of (a) the flat Pt and (b) $L_2$-ePt inserted in the brain at10 mV $s^{-1}$. Twisted RE denotes the Ag/AgCl wire, which is wound around the WEs.

In Figure 2-8, the *x*-axis in the cyclic voltammograms is for potential difference well controlled between the RE and WE. Most of in vivo electrochemical experiments reported to date employ two-electrode system, in which the distance between the two electrodes is rarely minded. More importantly, the electrochemical potential of the implanted WE is not defined in the extracellular media because of the absence of RE and/or *iR* drop due to the significant distance between WE and RE in the two electrode system. In this work, AgCl-coated Ag wire served as a RE fixing the electrochemical potential and its close proximity to the WEs in the three-electrode system allows precise control of electrochemical potential. Therefore, we were able to find and maintain the dc potential appropriate for minimal faradaic reaction otherwise undesired reaction and product may interfere during neural stimulation and sophisticated EIS experiments in the brain. Furthermore, flat and nanoporous Pt electrodes were fairly compared as exposed to almost the same electrochemical as well as biological environment.

The surface characteristic peaks of polycrystalline Pt in the brain appear to be smoothened (Figure 2-8(b)) in comparison to those in the buffer solution (Figure 2-7). The hydrogen adsorption and desorption peaks in the brain are not observed clearly, unlike in the buffer solution at similar pH. Presumably, this result stems

from contamination of the $L_2$-ePt surfaces by unidentified biochemical species in extracellular fluid. Nevertheless, the voltammetric behavior of the implanted Pt shows that electrochemistry in the brain works for both flat (Figure 2-8(a)) or nanoporous Pt electrodes (Figure 2-8(b)). The capacitance of $L_2$-ePt in the brain is much larger than flat Pt, indicating that the electric double layer is created correspondingly inside the nanopores and the real surface of nanoporous participates in the charging process (Figure 2-8(b)). The potential window ranges from –0.6 V to +0.8 V in good accordance with the literature[4], which is wide enough for neural stimulus. It also ensures safe EIS measurements without unwanted faradaic reactions by setting appropriate dc potential. Overall, voltammetric results show that the nanoporous Pt, $L_2$-ePt, reasonably behaves as a proper electrode implanted in animal tissues for the purpose of effective and safe stimulus and recording.

## 3.2. Change of electrode impedance in the brain

a

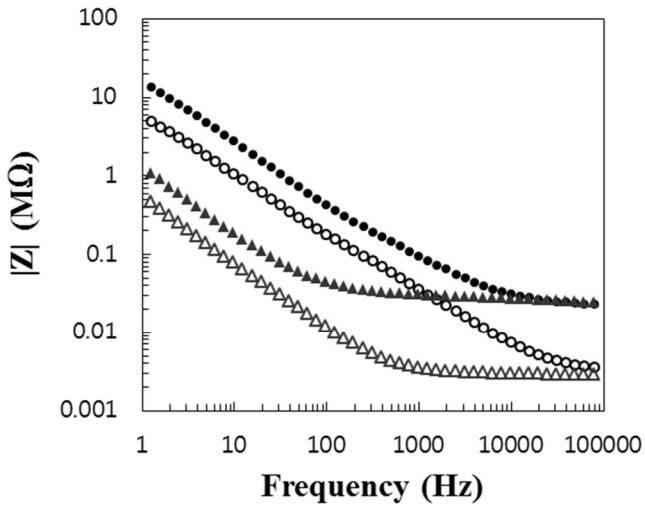


b

| | | $Z_{bulk}$ (kΩ) | $Z_e$ (kΩ) |
|---|---|---|---|
| Buffer Solution | Flat Pt | 2.67 | 32.22 |
| | $L_2$-ePt | 2.67 | 0.67 |
| Brain | Flat Pt | 14.00 | 78.00 |
| | $L_2$-ePt | 22.67 | 6.22 |

c

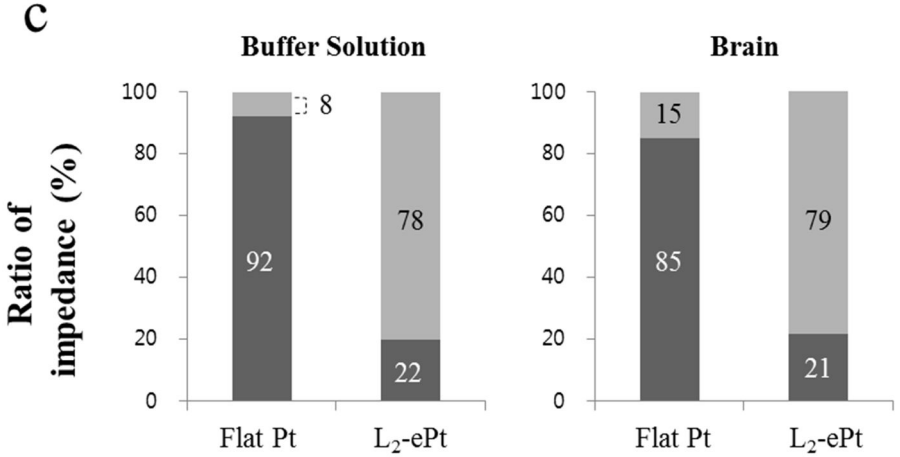

**Figure 2-9.** (a) Bode plots in the frequency range of 1 Hz-100 kHz at the flat Pt ( circle) and $L_2$-ePt (triangle) in the buffer solution (open) and in the brain (filled). (b) Impedance data for bulk solution and the electrode and (c) the ratio of bulk solution (gray) and electrode impedance (dark).

Figure 2-9(a) shows Bode plots of flat Pt and $L_2$-ePt in the buffer solution and the brain. From the cyclic voltammograms in Figure 2-8, we can find the potential range where faradaic current is minimal. We chose +0.2 V as the dc offset potential for non-faradaic condition. Such a condition was precisely maintained throughout the electrochemical experiments owing to the three electrode system with an Ag/AgCl wire in close vicinity to WEs. In the brain, $Z_{tot}$ values for both electrodes are higher than those in buffer solution, especially in the high frequency region. In low frequency region, the difference between the buffer solution and the brain is relatively small. As for $L_2$-ePt, this result implies that a shorter pulse than *ca*. 10 ms, corresponding to 100 Hz, should suffer from a considerable amount of extra impedance when implanted in the brain. Comparing the nanoporous electrode with flat one, the impedance of $L_2$-ePt is lower than flat Pt in the brain as well as in the buffer solution. The difference is significantly large at the low frequency up to 1 kHz. $Z_{tot}$ of the flat Pt and $L_2$-ePt eventually become similar at higher frequencies than 1 kHz. This means that we can exploit the low $Z_e$ of $L_2$-ePt, especially when applying an electric neural stimulus longer than 1 ms. It is worth to note that this

result offers a criterion for lower limit of pulse duration in order to benefit from nanoporous Pt for neural stimulation.

$Z_{tot}$ at extremely high frequencies indicates the bulk solution impedance ($Z_{bulk}$), coming from the neural tissue medium. Figure 2-9(b) tabulates $Z_e$ data that were calculated by subtracting the $Z_{bulk}$ from the $Z_{tot}$ at 1 kHz. In both the buffer solution and brain, $Z_e$ is undoubtedly higher than $Z_{bulk}$ for flat Pt whereas the ratio of $Z_e$ to $Z_{bulk}$ is inversed for $L_2$-ePt (Figure 2-9(c)). This shows how $L_2$-ePt can dramatically lower the impedance of the electrode itself. It is important that $Z_e$ of $L_2$-ePt implanted in the brain is substantially lower than flat Pt as it is in the buffer solution. Much less contribution of $Z_e$ to $Z_{tot}$ in $L_2$-ePt leads to less interference of the electrode itself in neural stimulating and recording. Therefore, the electric stimulus can reach a longer distance with less probable electrolysis, enabling effective stimulation without raising the external potential difference, even if the electrode is implanted at a place significantly apart from the targeted neuronal cell. Considering that it is not easy to implant the stimulating electrode at the place exactly where needed for neuromodulation therapy or experiments in practice, nanoporous electrode has its own value of extending the effective range of stimulation. This result also reveals that nanoporous structure of the electrode can be advantageous in recording neural signals coming from distant spots such as LFP because the low $Z_e$ allows detection to be less sensitive to the noise produced in vicinity to the electrode. $L_2$-ePt remarkably lowered $Z_e$ not only in the buffer

solution but also in the brain, explaining why and how nanoporous electrodes can contribute to neural stimulating and recording.

## 3.3. Comparison of the capacitances and influence of the tissue

a

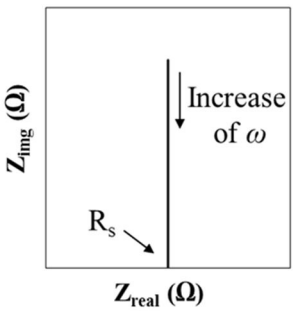


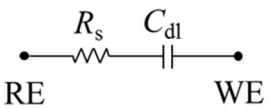


b

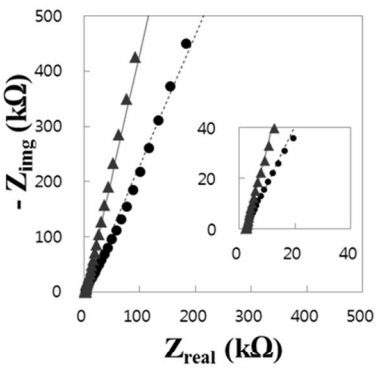


Buffer Solution

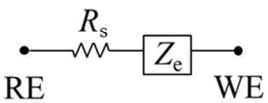


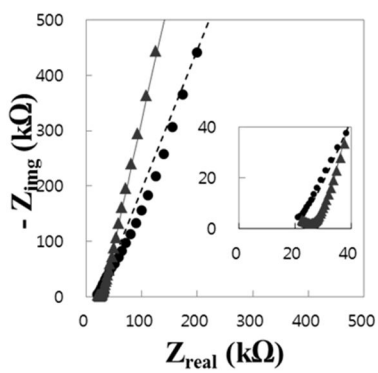


Brain

c

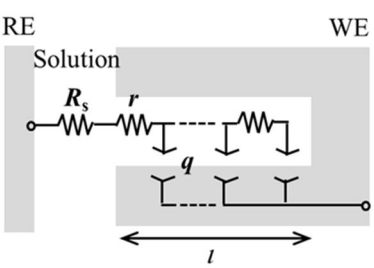


| | α |
|---|---|
| Flat Pt | 0.76 (± 0.02) |
| $L_2$-ePt | 0.86 (± 0.01) |

**Figure 2-10.** (a) Nyquist plots theoretically predicted from the dummy circuit consisting of a resistor and a capacitor in series and (b) Nyquist plots from the experiments in the buffer solution and the brain under non-faradaic conditions. In (b), the data from flat Pt (circle) and $L_2$-ePt (triangle) were fitted using the equivalent circuit with constant phase element based on transmission line model (TLM). The curves fitted to the data from flat Pt are dashed lines and those from $L_2$-ePt are solid lines, respectively. Insets show the magnified view in the high frequency domain. The dc offset potential is +0.2 V and the amplitude of alternating current potential is 10 mV. (c) Adopting the TLM for fitting (left), we calculated α values in the brain (in table on the right).

a

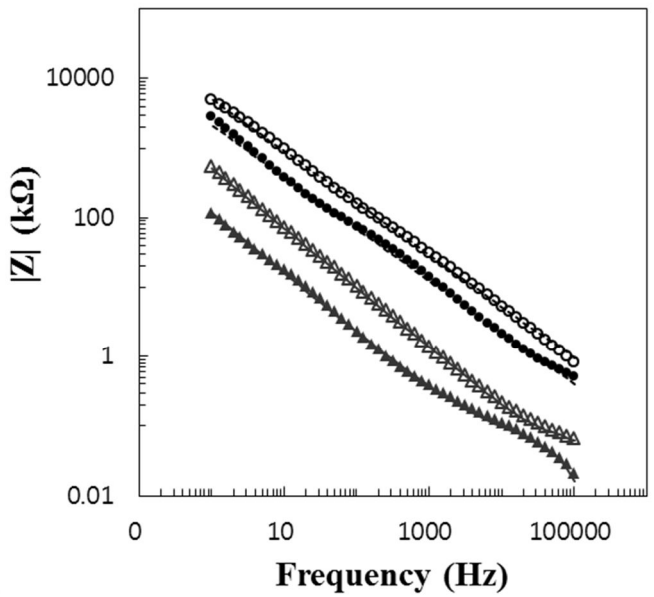
10000
100
1
0.01
|Z| (kΩ)
0
10
1000
100000
Frequency (Hz)

b

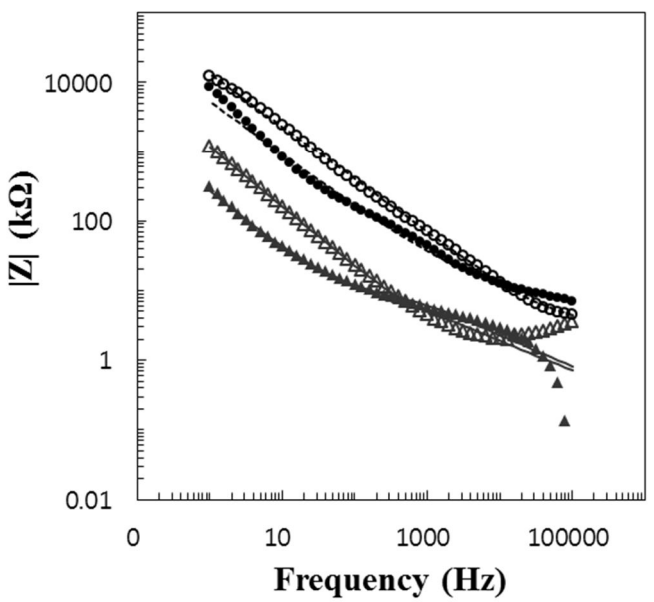
10000
100
1
0.01
|Z| (kΩ)
0
10
1000
100000
Frequency (Hz)

**Figure 2-11.** Bode plots from flat Pt (circle) and $L_2$-ePt (triangle) in (a) buffer solution and (b) brain. The $|Z|$ of a y-axis in the Bode plots indicates $Z_{Re}$ (closed) and $Z_{Im}$ (open) values $Z_{RE}$ (closed), $Z_{Im}$ (open). The $Z_{Re}$ values in the Bode plots were corrected with the solution resistances. The data were fitted based on an equivalent circuit for TLM presented in Figure 2-10(c). The curves fitted to the data from flat Pt are dashed lines and those from $L_2$-ePt are solid lines.

To analyze the impedance spectra and extract information, we adopted TLM, which is widely used for porous electrode systems[39] in Figure 2-10(c), and the detailed fitting procedures are described in Supporting Information. If the assumption of non-faradaic condition is valid, the electrode should be regarded as a simple capacitor. With a serial resistance such as solution resistance, Nyquist plot should simply follow a vertical line in Figure 2-10(a).

The experimental results from flat Pt and $L_2$-ePt are linear series of data slightly tilted as shown in Figure 2-10(b). The deviation from the ideal behavior implies that other electrochemical processes than merely charging are involved in the whole system. The capacitance element in the equivalent circuit (Figure 2-10(a)) cannot be expressed merely by an ideal capacitance ($C_{dl}$). Thus, we introduced a constant phase element (CPE) that is conventionally used for empirical models of electrode-electrolyte interface, e.g. interpreting non-ideal capacitive properties of metal electrodes.[40] In this study, the CPE is designated by $Z_e$ in Figure 2-10(b)

instead of $C_{dl}$. Figure 2-10(b) shows that the slope of $L_2$-ePt is steeper than flat Pt not only in the buffer solution but also in the brain. This means that the $L_2$-ePt behaves more like an ideal capacitor whether it is implanted or not. In the equivalent circuit (Figure 2-10(c)), $r$ is the electrolyte resistance per unit of length in the pores, $l$ is the film thickness, $q$ is the CPE, and α is a function of the phase angle $\phi$ with the relation of $\alpha = \phi / (\pi / 2)$. From α value obtained by fitting the experimental data, we can quantitatively determine the term for CPE (See chapter 2.5 in experimental methods). α value closer to unity indicates that the system can be successfully represented by the ideal capacitor. The average α values from three independent measurements in Figure 2-10(c) are clearly dissimilar between flat Pt and $L_2$-ePt in terms of deviation from pure capacitive character. The α values can be obtained from the Bode plots as well and are consistent with those from the Nyquist plots (Figure 2-11 and chapter 2.6 in experimental methods). $L_2$-ePt created electrochemical system closer to the ideal capacitance, suggesting its ability to minimize the side reactions, i.e. unwanted faradaic reactions, and thus enable us to record neural signals and stimulate the target cells or tissues more effectively.

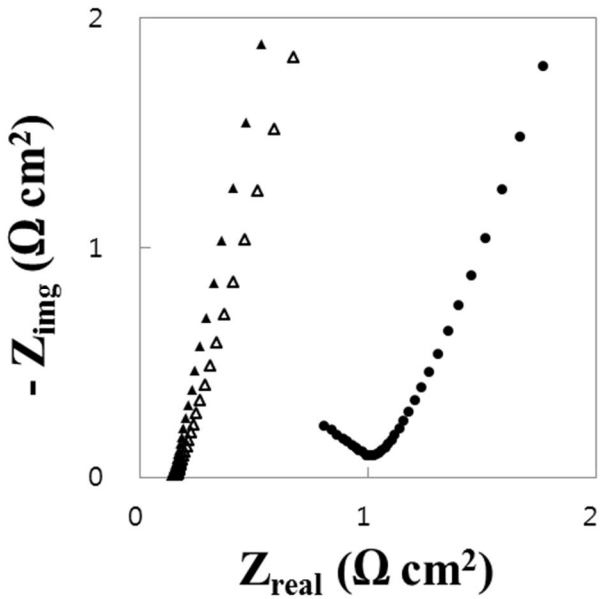


**Figure 2-12.** Nyquist plots in the buffer solution before (closed triangle) and after (opened triangle) implantation and in the brain (closed circle).

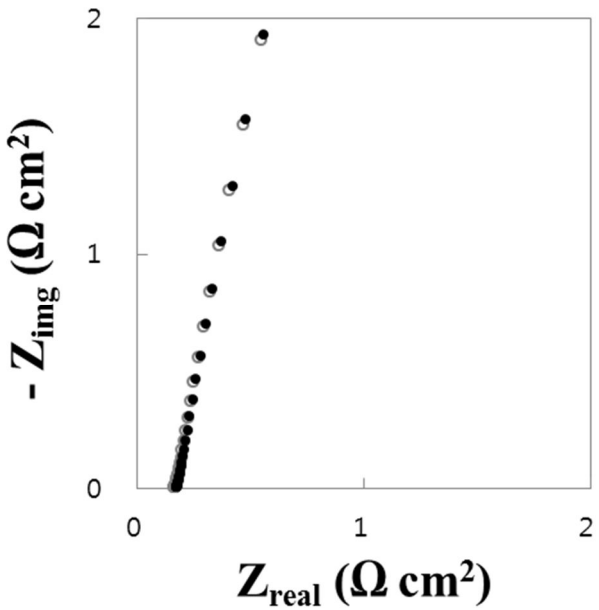


**Figure 2-13.** Nyquist plots in the buffer solution (opened circle) and bovin serum albumin in the buffer solution (closed circle).

Inset plots in Figure 2-10(b) display the Nyquist plots in the high frequency region. When implanted in the brain, the real impedance ($Z_{real}$) values for both flat Pt and $L_2$-ePt increase as seen in the *x*-intercepts of the curves. It is not surprising that $Z_{bulk}$ in the brain is larger than that in aqueous pure electrolyte. It is probable that the electrode surface was passivated or irreversibly adsorbed by insulating species. To investigate the cause of this result, we put the electrode, which had been implanted in the brain, into the buffer solution and conducted an identical impedometric experiment (Figure 2-12). Regardless of the history of implantation,

electrochemical behavior was recovered reproducibly for both flat and nanoporous electrodes to give the results as presented in Figure 2-10(b). Fresh electrodes were immersed in the buffer solution containing 0.2 mg/ml of bovine serum albumin to see if any irreversible adsorptive processes take place due to the presence of abundant proteins (Figure 2-13). There was no significant permanent adsorption of proteins, and no intercept shift of $Z_{real}$ was observed in the Nyquist plots.

For $L_2$-ePt implanted in the brain, the Nyquist curve in high frequency domain deviates from linearity and sagging. Biological media such as animal tissues are expected to impose nonlinear impedance on the circuit. Considering the numerous cells enclosing electrolytes in their own cytosols, it is presumably possible that external electric field brings about inductive ion current. Low $Z_e$ of $L_2$-ePt should make potential gradient reach out farther so that much more cells respond to the electric potential perturbation. This could be a potential explanation for the lowering of imaginary impedance in the high frequency regime. For now this is difficult to be quantitatively proved, but we can infer that such an impedance behavior should be observed in the two electrode system, in which they are implanted in animal tissue and considerably apart from each other, when exerting electric potential modulation of the time scale shorter than ms.

# 4. Conclusions

Invasive electric neuromodulation is advancing with increasing attention in terms of remarkable therapeutic benefits for patients as well as neuroscientific interest. Although electrochemistry is obviously involved and possibly influences on the performance of electrodes implanted, what happens near the electrode in animal tissues remains obscure. Owing to abundant electrolytes in the tissue, extracting analytical information from regions close to the electrode should be possible without critical problems. However, practical neural stimulation and recording do not concern much about the region within several tens of nm from the implanted working electrode. Tremendous demands of electrochemistry in animal tissues is rising in recording LFP coming from distant sources, and stimulating cells located somewhere between the implanted two electrodes, possibly away from the electrode surface. In these regards, it is a clever strategy to lower the impedance of electrode-tissue interface. Nanoporous electrode is attractive because nothing but modifying surface geometry is required to realize the idea. In this work, we investigated the characteristic electrochemical behavior of nanoporous electrodes in detail by EIS as well as conventional voltammetry in a rat embryo brain for the first time. We employed $L_2$-ePt as a nanoporous electrode because it is an outstanding candidate due to its extremely small pores without electrical double layer overlapping, uniformity, and mechanical stability outdoing Pt black. The comparison study with flat Pt under carefully controlled condition showed that $L_2$-ePt successfully worked as an electrode in the brain and maintained the nanoporous

effect. As expected, $L_2$-ePt remarkably suppressed the electrode impedance to behave like a pseudo-ideal capacitive probe with minimal unwanted faradaic reaction as well as electrode passivation. In addition, EIS analysis showed that nanoporous effect is subject to frequency range, having an implication that the lessons from this study need to be considered in determining the parameters for neural stimulation using nanoporous electrodes, e.g. pulse duration. Further in vivo electroanalytical approach with nanoporous electrodes is in demand to expedite the progress of neural recording and stimulation for more sophisticated electric therapy and prosthetic devices.

## 5. References


(1) Andrews, R. J. *Ann. N.Y. Acad. Sci.* **2003,** *993*, 1–13.

(2) Andrews, R. J. *Ann. N.Y. Acad. Sci.* **2003,** *993*, 14–24.

(3) Bear, M. F.; Connors, B. W.; Paradiso, M. A. *Neuroscience exploring the brain*; 3th ed.; Lippincott Williams & Wilkins.

(4) Cogan, S. F. *Annu. Rev. Biomed. Eng.* **2008**, *10*, 275-309.

(5) Novak, J. L.; Wheeler, B. C. *Brain Res.* **1989**, *497*, 223–230.

(6) Nisch, W.; Bock, J.; Egert, U.; Hammerle, H.; Mohr, A. *Biosens. Bioelectron.* **1994**, *9*, 737–741.

(7) Nordhausen, C. T.; Rousche, P. J.; Normann, R. A. *Brain Res.* **1994**, *637*, 27-36.

(8) Cahill, P. S.; Walker, Q. D.; Finnegan, J. M.; Mickelson, G. E.; Travis, E. R.; Wightman, R. M. *Anal. Chem*. **1996**, *68*, 3180-3186.

(9) Garris, P. A.; Collins, L. B.; Jones, S. R.; Wightman, R. M. *J. Neurochem.* **1993**, *61*, 2, 637-647

(10) Ewing, A. G.; Wightman, R. M.; Dayton, M. A. *Brain Res.* **1982**, *249*, 361-370.

(11) Ha, Y.; Sim, J.; Lee, Y.; Suh, M. *Anal. Chem.* **2016**, *88*, 2563-2569.

(12) Robinson, D.A. *Proceedings of the IEEE* **1968**, *56* (6), 1065-1071.

(13) Thomas, C. A.; Springer, P. A.; Loeb, G. E.; Berwald-Netter, Y.; Okun, L. M. *Experimental Cell Research* **1972**, *74* (1), 61-66.

(14) Butson, C. R.; McIntyre, C. C. *Clin Neurophysiol.* **2005**, *116* (10).

(15) Joucla, S.; Yvert, B. *PLoS ONE* **2009**, *4(3)*, e4828 .

(16) Butson, C. R.; Maks, C. B; McIntyre, C. C. *Clinical Neurophysiology* **2006**, *117*, 447-454.

(17) Miocinovic, S.; Lempka, S. F.; Russo, G. S.; Maks, C. B.; Butson, C. R.; Sakaie, K. E.; Vitek, J. L; McIntyre, C. C. *Experimental neurology* **2009**, *216*, 166-176.

(18) Lempka, S. F.; Miocinovic, S.; Johnson, M. D.; Vitek, J. L.; McIntyre, C. C. *J. Neural. Eng.* **2009**, 6, 046001.

(19) Williams, J. C.; Hippensteel, J. A.; Dilgen, J.; Sahin, W.; Kipke, D. R. *J. Neural Eng.* **2007**, *4*, 410-423

(20) Mercanzini, A.; Colin, P.; Bensadoun, J-C.; Bertsch, A.; Renaud, P. *IEEE Transaction Biomedical Engineering* **2009**, *56*, 7, 1909-1918.

(21) Polikov, V. S.; Tresco, P. A.; Reichert, W. M. *J. Neurosci. Methods* **2005**, *148*, 1-18.

(22) Rousche, P. J.; Normann, R. A. *J. Neuroscience Methods* **1998**, *82*, 1-15.

(23) Liu, X.; McCreery, D. B.; Carter, R. R.; Bullara, L. A.; Yuen, T. G. H.; Agnew, W. F. *IEEE Transaction on Rehabilitation Engineering* **1999**, *7*, 3, 315-326.

(24) Williams, J. C.; Rennaker, R. L.; Kipke, D. R. *Brain Research Protocols* **1999**, *4*, 303-313.

(25) Ignatius, M. J.; Sawhney, N.; Gupta, A.; Thibadeau, B. M.; Monteiro, O. R.; Brown, I. G. *J Biomed Mater Res* **1998**, *40*, 264–274 .

(26) Cui, X. Y.; Lee, V. A.; Raphael, Y.; Wiler, J. A.; Hetke, J. F.; Anderson, D. J.; *J Biomed Mater Res* **2001**, *56*, 261–72.

(27) Cui, X. Y.; Martin, D. C. *Sens Actuators A-Phys* **2003**, *103*, 384–94.

(28) Yang, J. Y.; Martin, D. C. *Sens Actuators A-Phys* **2004**, *113*, 204–11.

(29) Heim, M.; Yvert, B.; Kuhn, A. *Journal of Physiology-Paris* **2012**, *106*, 137-145.

(30) Park, S.; Song, Y. J.; Boo, H.; Chung, T. D. *J. Phys. Chem. C* **2010**, *114* (19), 8721-8726.

(31) Park, S.; Lee, S. Y.; Boo, H.; Kim, H.-M.; Kim, K.-B.; Kim, H. C.; Song, Y. J.; Chung, T. D. *Chem. Mat.* **2007**, *19* (14), 3373-3375.

(32) Part, S.; Song, Y. J.; Han, J-H.; Boo, H.; Chung, T. D. *Electrochimica Acta* **2010**, *55*, 2029-2035.

(33) Bae, J. H.; Kang, C. M.; Choi, H.; Kim, B. J.; Jang, W.; Lim, S. Y.; Kim, H. C.; Chung, T. D. *Anal. Chem.* **2015**, *87*, 2443-2451.

(34) Heim, M.; Rousseau, L.; Reculusa, S.; Urbanova, V.; Mazzocco, C.; Joucla, S.; Bouffier, L.; Vytras, K.; Bartlett, P.; Kuhn, A.; Yvert, B. *J Neurophysiol* **2012**, *108*, 1793-1803.

(35) Bard, A. J.; Faulkner, L. R. *Electrochemical Methods fundamentals and application*, 2th ed, pp22~27.

(36) Levie, R. D. *Electochim. Acta* **1963**, *8*, 751-780.

(37) Robinson, D. B.; Wu, C. A. M.; Ong, M. D.; Jacobs, B. W.; Pierson, B. E. *Langmuir* 2010, 26 (9) 6797-6803

(38) Trasatti, S.; Petrii, O. A. *J. Electroanal. Chem.* **1992**, *327* (1-2), 353-376.

(39) Elliott, J. M.; Owen, J. R. *Phys. Chem. Chem. Phys.* **2000**, *2* (24), 5653-5659.

(40) McAdams, E. T.; Lackermeier, A.; McLaughlin, J. A.; Macken, D.; Jossinet, J. *Biosen. Bioelectron.* **1995**, *10*, 67-74.

# PART 3.

## Specific Designed EC-microprobe for EC reaction

# 1. Introduction

*In situ* investigation of chemical/electrochemical or biological events occurring at interfaces between aqueous media and various types of surface have long attracted attention. Needless to say, monitoring of molecular species, involved in the reactions occurring at heterogeneous interfaces, is increasingly important for producing better rechargeable batteries, solar cells, and fuel cells, understanding biological secretions, and many more applications.[1-7] High throughput screening of organic and inorganic catalysts[8] as well as biological functional units immobilized on surfaces[9] are practical topics that require *in situ* analytical tools operating in aqueous media.

A scanning electrochemical microscope (SECM) using an ultramicroelectrode (UME) is a representative tool for this purpose.[3-4] However, its limited capacity for identifying molecular characteristics, especially for electro-inactive species, remains a critical problem that current SECM should address. Combining electrochemistry with other techniques, for example, atomic force microscopy (AFM) or near-field scanning optical microscopy (NSOM), has led to significant advances in interfacial science.[1]

In particular, surface-enhanced Raman scattering (SERS), which allows Raman spectroscopy of reactions in water by enhancing the signal intensity, has been attracting keen interest as a convenient and powerful tool in combination with electrochemistry.[10-12] However, SERS requires strict conditions; working on only a

limited number of substrates such as coinage metals (Au, Ag, and Cu)[11-12] and rough surfaces,[13] thus precluding versatile applications. Furthermore, the surface morphology and dimension of previously reported probes were not standardized and thus were poorly reproducible as not only SERS substrates but also UMEs. Such problems in obtaining reproducible spectra have critically hindered the development of reliable analytical systems that can provide Raman spectroscopic as well as electrochemical information simultaneously.[14]

Since the first experimental report,[15-18] tip-enhanced Raman spectroscopy (TERS) has evolved the capacity to acquire Raman spectra on smooth,[18] single crystalline,[19] and even non-conducting surfaces.[20-22] Advances in TERS technology have made considerable contributions to Raman spectroscopic studies on more general substrates.[14] Recently, significant contributions were made, including the potential to insert a multifunctional probe into a living cell to obtain both electrochemical and spectroscopic information about intracellular molecular species[23] and the development of a gap-mode-free AFM-SERS probe with precisely controlled hot spots.[24]

In the present work, we suggest a new EC-SERS probe that has a gold μ-shell with a carefully tuned surface at the end of the probe. The proposed probe consists of stable and well-defined parts that could be quickly and reproducibly assembled to provide both electrochemical and SERS responses reliably. The gold μ-shell in this probe has numerous hot spots on its surface so as to induce sufficiently strong SERS.[25]

# 2. Experimental Methods

## 2.1. Reagents

Tetrakis (hydroxymethyl) phosphonium chloride (THPC) solution, sodium hydroxide, gold (III) chloride trihydrate ($HAuCl_4$), potassium carbonate, and formaldehyde were purchased form Aldrich. Amine-terminated polystyrene beads ($PS\text{-}NH_2$, *ca.* 1.8 μm in diameter) was from Bangs Laboratories, Inc. These materials were used to fabricate a SERS-active gold μ-shell. To fabricate the Ru-coated micropipette, a borosilicate glass capillary (GC 150F-10, Harvard part No. 30-0057), a $CO_2$ laser-based micropipette puller (Sutter Instruments Inc., P-2000), Bis(ethylcyclopentadienyl) ruthenium, and a showerhead-type ALD system (GENI-MP 1000, ASM-Genitech, Inc.) were used. For permanetly sticking a gold μ-shell to the end of the micropipette, potassium tetrachloroaurate (III) hydrate ($KAuCl_4$, Strem Chemicals, USA), potassium ferrocyanide solution ($K_4[Fe(CN_6)]$, Junsei Chemical Co., Ltd., Japan) were filtered.

## 2.2. Preparation of the in-situ EC-SERS probe

### 2.2.1. Fabrication of a SERS-active Gold μ-shell[25]

SERS-active gold μ-shells were sophisticatedly engineered by electroless deposition procedure. Colloidal gold nanoparticles (AuNPs, *ca*. 2-3 nm in diameter) were synthesized by the process in the literature.[26] Tetrakis

(hydroxymethyl) phosphonium chloride (THPC) solution was prepared by adding 12 μL of 80 % THPC (0.067 mmol, Aldrich) in 1 mL of water. 0.5 mL of 1 M sodium hydroxide (Aldrich) in water and 1 mL of THPC solution were added to 45 mL of deionized water (Barnstead Nanopure, Thermo Fisher Scientific Inc.). This reaction mixture was stirred for 5 min by a vortex mixer (Vortex-2 Genie, Model G-560, Scientific Industries) and 2.0 mL of 1 % gold (III) chloride trihydrate ($HAuCl_4$, Aldrich) in water was added to above solution. This mixture was stirred until brown color was appeared and the solution was stored in refrigerator at 4 °C when not used immediately. Amine-terminated polystyrene beads (PS-$NH_2$, *ca*. 1.8 μm in diameter, 10 % dispersed in water, Bangs Laboratories, Inc.) were washed with water. For this cleaning process, 0.5 mL of PS-$NH_2$ solution and 5 mL of water were added in a centrifuge tube. The tube was centrifuged at 2000 rpm for 5 min and the supernatant was decanted and 5 mL of water was added. This process was repeated several times and the PS-$NH_2$ was dried in a vacuum oven overnight. 0.05 g PS-$NH_2$ and 0.5 mL water were added in a centrifuge tube to prepare 10 % PS-$NH_2$ dispersed in water. 5 mL of colloidal AuNPs were added to 0.5 mL of 10 % PS-$NH_2$ solution. After 2 h, the AuNPs were adhered to PS-$NH_2$. This mixture solution (PS-$NH_2$/AuNP) was cleaned by the sequential processes of water using centrifugation, decanting and adding water. Next, PS-$NH_2$/AuNP was dispersed again in 5 mL water and stored in refrigerator at 4 °C. In order to prepare an Au plating solution, 15 mL of 1 % $HAuCl_4$ solution was added to 1000 mL of 0.18 mmol potassium carbonate (Aldrich) solution in water and stirred until the solution

was to be colorless. A 20 mL of the Au plating solution and 140 μL of formaldehyde (solution in water, 37 wt. %, Aldrich) were added to 1 mL of PS-$NH_2$/AuNP solution. The mixture was stirred vigorously, and a dark blue-colored suspension was obtained within 2 min. This solution was centrifuged at 2000 rpm for 5 min, and the supernatant was decanted. After adding 20 mL of water, the solution was centrifuged at 2000 rpm for 5 min and the supernatant was decanted. This electroless plating process was repeated 20 times for preparing electro- and SERS-active gold μ-shell. (Figure 3-1)

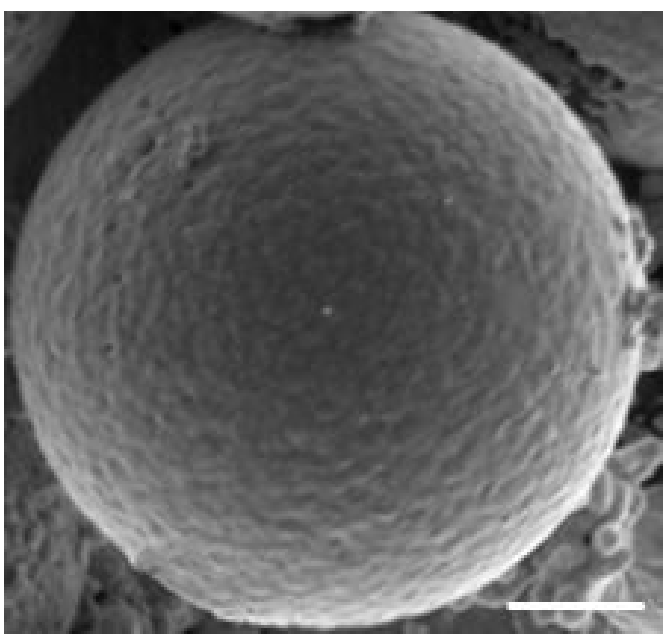

**Figure 3-1.** FE-SEM image of a EC-SERS gold μ-shell which has been plated 20 times. The scale bar in the lower right denotes 0.5 μm.

### 2.2.2. Preparation of a Ru Coated Micropipette

A borosilicate glass capillary (GC 150F-10, Harvard part No. 30-0057) was rinsed with acetone (99.5 %, Daejung), methanol (99.5 %, Daejung) and deionized water. By using $CO_2$ laser-based micropipette puller (Sutter Instruments Inc., P-2000), we made a glass micropipette with *ca*. 1.8 μm diameter. The pulling parameters were Line 1 (Heat: 450, Fil: 430, Vel: 200, Pull: 0), Line 2 (Heat: 450, Fil: 430, Vel: 200, Pull: 0), Line 3 (Heat: 450, Fil: 430, Vel: 200, Pull: 0) and Line 4 (Heat: 450 , Fil: 430 Vel: 128, Pull: 50). Ru thin film was deposited both inside and outside surfaces of the micropipette by an atomic layer deposition (ALD) method. ALD process was conducted using a showerhead-type ALD system (GENI-MP 1000, ASM-Genitech, Inc.) at a deposition temperature of 300 °C and a working pressure of 3 Torr. Bis(ethylcyclopentadienyl) ruthenium, oxygen, and Ar were introduced as a precursor, a reactant, and a carrier/purge gas, respectively. To deliver the Ru precursor, Ar with a flow rate of 100 sccm (standard cubic centimeter per minute) was used as the carrier gas. One ALD cycle consisted of Ru precursor pulsing (40 s), Ar purge (10 s), oxygen reactant pulsing (20 sccm for 10 s), and Ar purge (5 s). By repeating 1,000 ALD cycles, 50 nm thick Ru film was uniformly coated at both the inside and outside of the micropipettes. In order to remove outside Ru of the micropipette, the micropipette was put in the Ru etching solution (Ru etchant Ru-44, Transene Company Inc.) for 3 min while positive pressure was applied through the micropipette to protect the inside Ru.

### 2.2.3. Permanently Sticking a Gold μ-shell to the End of the Ru Coated Micropipette

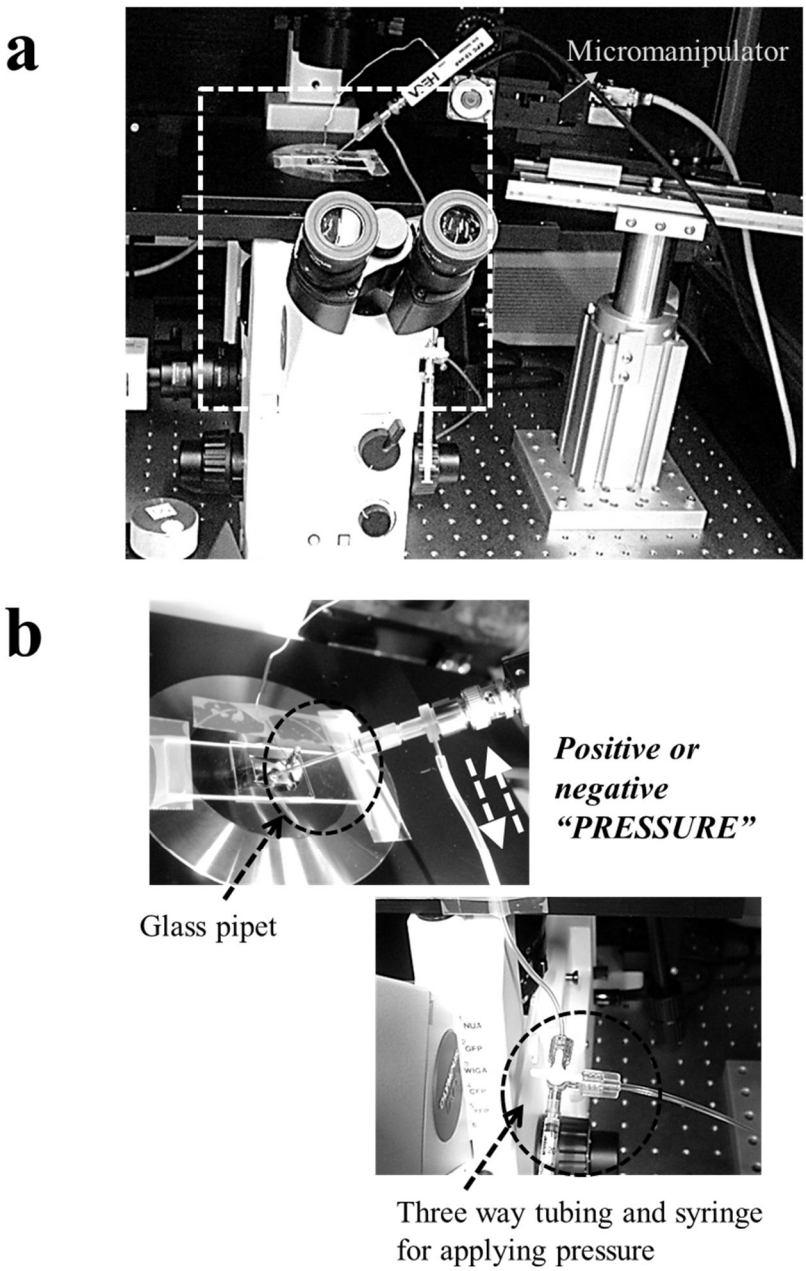

**Figure 2-2.** (a) a probe micromanipulating system with (b) negative or positive pressure.

All solutions were filterd by filtering unit (*ca.* 0.22 μm pore diameter, Millipore, USA), because the end of the micropipette was easily blocked by unknown particles. 1 % of potassium tetrachloroaurate (III) hydrate ($KAuCl_4$, Strem Chemicals, USA) solution in water used as a gold precursor and 0.25 M of potassium ferrocyanide solution ($K_4[Fe(CN_6)]$, Junsei Chemical Co., Ltd., Japan) in water used as a reducing agent. When we selected the gold μ-shell having a good SERS activity using an inverted micoscope (1X71, Olympus, Japan), the gold μ-shells directly on to the coverslip (Marienfeld, Germany) give a favorable position to distinguish them. For this, The gold μ-shells, which were dispersed in water, were dropped on a coverslip and evaporated in advance of adding $KAuCl_4$ solution. Through the inverted micoscope, we chose one of the gold μ-shells in $KAuCl_4$ solution. By using a narrow format micromanipulator (Model MP265/M and MPC-200, sutter Instruments Co., USA), the Ru coated micropipette, which was filled with the $KAuCl_4$ solution, was came close to the gold μ-shell. To prevent blocking of the end of the micropipette by unknown species, we applied a positive pressure when the micropipette was entered the solution and removed the pressure in the vicinity of the gold μ-shell. After moving the micropipette adjacent to the gold μ-shell, the gold μ-shell was trapped to the end of the micropipette by applying a

negative pressure. Figure 2-2(a) shows probe manipulating system with negative and positive pressure. Using three way tubing and a syringe, we could apply the pressure (Figure 2-2(b)). At that moment, we applied the strong negative pressure so that the μ-shell didn't fall off the micropipette. Excess water was added to the drop of the gold μ-shells/$KAuCl_4$ solution in order to get rid of the diluted $KAuCl_4$ solution (Figure 3-3(a)-(b)). This process should be repeated 5 times to remove the gold precursor. During exchanging a solution, the micropipette with the gold μ-shell should be kept in a liquid phase, because the strong surface tension of the meniscus should easily separate the gold μ-shell from the micropipette. And then, 0.25 M $K_4[Fe(CN_6)]$ solution as a reducing agent was also gently added and the negative pressure was eliminated (Figure 3-3(c)). From the reducing agent, the electroless deposition was occurred with time in Figure 3-4(b). After 2 h, the gold μ-shell was permanently attached to the end of the micropipette (Figure 3-4(a)). The completed EC-SERS probe was rinsed by water and $KAuCl_4$ solution in the micropipette was removed.

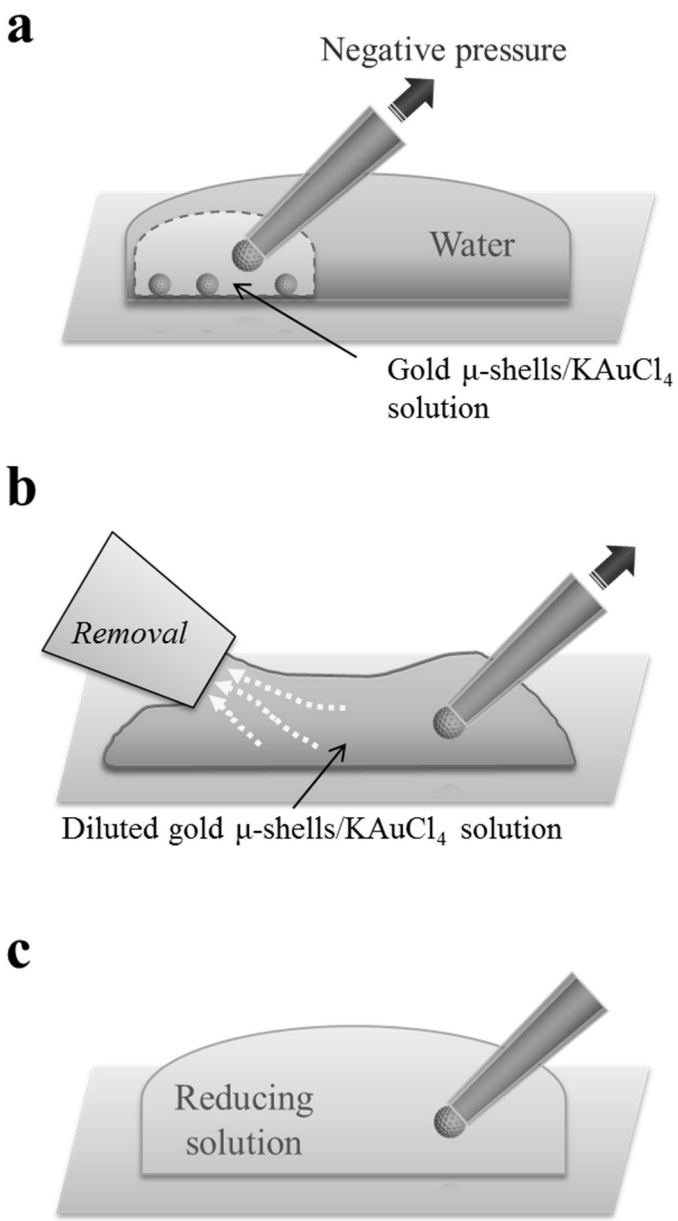


**Figure 3-3.** Schematic illustrations of the process to exchange solutions. (a) Adding the excess water to the micropipette with the gold μ-shell in the gold μ-shells/$KAuCl_4$ solution. (b) Removing the diluted $KAuCl_4$ solution. (c) For

electroless plating process, add the reducing solution to the micropipette with the gold μ-shell in water.

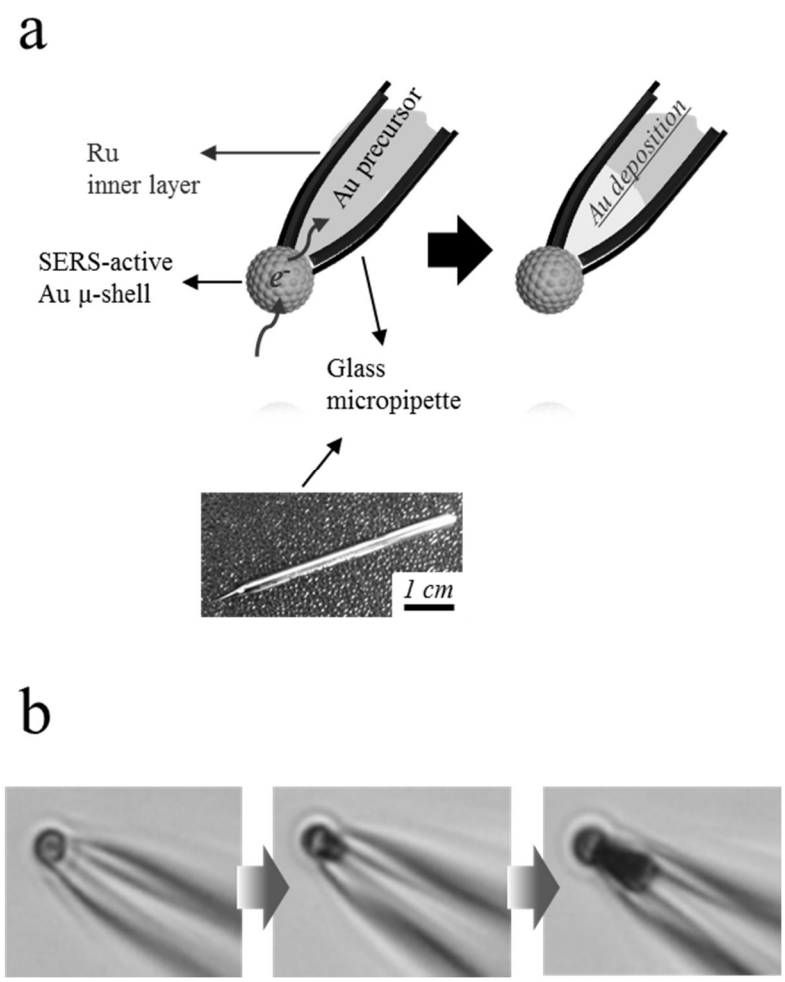


**Figure 3-4.** (a) Schematic and (b) Optical microscope images of a gold μ-shell to the end of a micropipette according to the electroless deposition procedure. The scale bars denote 5 μm.

## 2.3. Electrochemical and Optical Measurements

Cyclic voltammogram curves were measured using an electrochemical analyzer (CHI-750 A, CH Instruments Inc., Austin, TX). SERS spectrum were obtained using a homemade Ramboss Micro-Raman system spectrometer with a 632.8 nm line from a 3 mW He/Ne laser (LASOS Lasertechnik GmbH, USA) as a excitation source.

## 2.4. Evaluation of the Functions of the in-situ EC-SERS probe

The Field-Emission Scanning Electron Microscope (FE-SEM) image was obtained by SUPRA 55 VP (Carl Zeiss, Germany) using electron beam power (2.0 kV). Cyclic voltammogram curves were measured using an electrochemical analyzer (CHI-750 A, CH Instruments Inc., Austin, TX). Reference electrode was Ag/AgCl (BASi) and counter electrode was platinum wire (Aldrich). A 5 mM aqueous solution of hexaammineruthenium (III) chloride and 0.1 M KCl was used. In faraday cage (UA/CHI 200, CH Instrument, USA), electrochemical measurement was carried out under nitrogen atmosphere. The voltage was scanned between 0.1 V and - 0.4 V with scan rate of 0.03 V $s^{-1}$. SERS spectrum were obtained using a homemade Ramboss Micro-Raman system spectrometer with a 632.8 nm line from a 3 mW He/Ne laser (LASOS Lasertechnik GmbH, USA) as a

excitation source. The diameter of the laser focus was *ca*. 2 μm through a 100 x objective lens. The Raman scattering was detected using a TE cooled (- 50 ℃) CCD camera (1024 x 127 pixels, Andor, iDus DV 401). The Calibration of the spectrometer was achieved using the Raman band of a silicon wafer at *ca*. 520 $cm^{-1}$ to normalize the peak intensities of the adsorbates on the gold μ-shell. To obtain the SERS signal from the EC-SERS probe modified with 4-nitrobenzenethiol (NBT, 80 %, Aldrich), the probe was soaked in 10 mM of NBT solution in absolute ethanol (≥ 99.9 %, Merck) for 17 h at 4 ℃. NBT modified probe was washed by ethanol and water. After evaporating water, SERS spectrum was obtained by focusing the laser beam through an optical microscope.

## 2.5. Electrochemical Surface Area Calculation of the EC-SERS probe

The area of the electrochemically active surface was calculated from the diffusion-controlled steady state current. As our probe had globular shape, we used the equation of the steady state current $i_{ss}$ of the spherical or hemispherical UME.[27] The steady state current $i_{ss}$ of the spherical UME is,

$$i_{ss} = 4\pi nFD_0C_0^* r_0 \quad (1)$$

The steady state current $i_{ss}$ of the hemispherical UME is,

$$i_{ss} = 2\pi nFD_0C_0^* r_0 \quad (2)$$

Applying 3 nA of the $i_{ss}$ in Figure 3-8(c) and a diffusion coefficient[28], $D_0$, of 6.0

$\times 10^{-6}$ $cm^2$ $s^{-1}$ to the equations of spherical and hemispherical UME, we obtained the 1.6 μm and 3.3 μm of diameter respectively. The discrepancy occurs compared to the 2 μm diameter of a gold μ-shell measured from FE-SEM image (Figure 3-8(b)) because the shape of the probe is in the middle between sphere and hemisphere.

## 2.6. *In situ* Electrochemical SERS Monitoring of NBT reduction and Py Adsorbed on the EC-SERS probe

The spectra were recorded from the active site of the probe which was focused by 632.8 nm laser with 4 μm diameter through a 50 x objective lens. The intensity of laser was 3 mW and integration time was 10 s. This experiment was performed in a homemade faraday cage and the EC-SERS probe was placed in a homemade EC-SERS cell using micromanipulator. To demonstrate *in situ* electrochemical SERS monitoring, we conducted two different potential dependent SERS expeirment. First, we observed the electrochemical reduction of NBT modified on the probe in 0.1 M $H_2SO_4$ solution. Second, pyridine (Py, Sigma-Aldrich) monitored in 0.1 M of pyridine solution in 0.1 M of sodium perchlorate ($NaClO_4$, ≥ 98.0 %, Sigma-Aldrich). All experimental solution were degassed with nitrogen for 1 h before an experiment. The nitrogen gas was passed over the top of the solution during the experiment. For NBT reduction, potential dependent SERS spectrum were obtained at + 0.45 V, - 0.35 V, and -0.5 V by using the electrochemical

analyzer. For Py experiment, the voltage was scanned between + 0.4 V and - 0.8 V with scan rate of 0.02 V $s^{-1}$ by using the electrochemical analyzer.

a

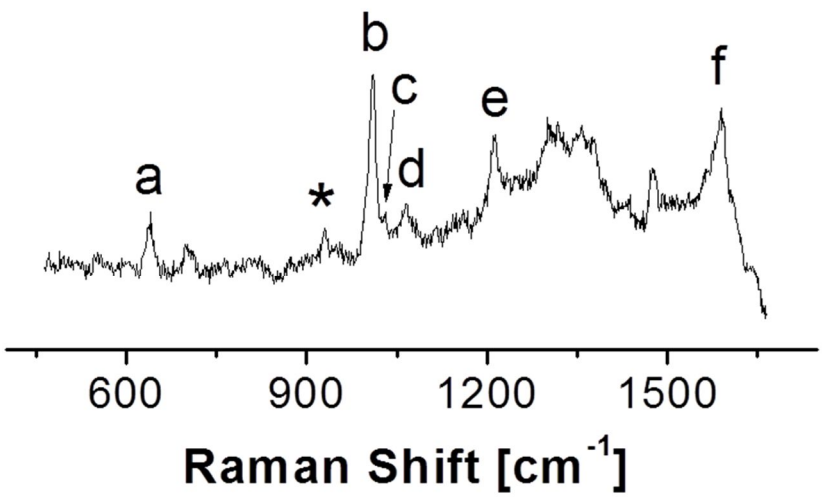


b

| label | SERS peak ($cm^{-1}$) | Vibration mode | Vibration type |
|---|---|---|---|
| a | 634 | $\nu_{6a}$ | symmetric |
| b | 1008 | $\nu_1$ | Ring breathing mode |
| c | 1029 | $\nu_{12}$ | C-H in-plane deformation |
| d | 1066 | $\nu_{18a}$ | C-H in-plane deformation |
| e | 1216 | $\nu_{9a}$ | C-H in-plane deformation |
| f | 1592 | $\nu_{8a}$ | Ring stretching |

**Figure 3-5.** (a) A SERS spectrum of Py adsorbed on the EC-SERS probe in 0.1 M Py solution in 0.1 M $NaClO_4$ at -0.6 V applied potential. (b) The detailed peak assignment of (a) which agrees exactly with reported previously SERS spectra.[10,38]

# 3. Results and Discussion

## 3.1. Preparation of Electrochemical SERS Monitoring System and EC-SERS probe

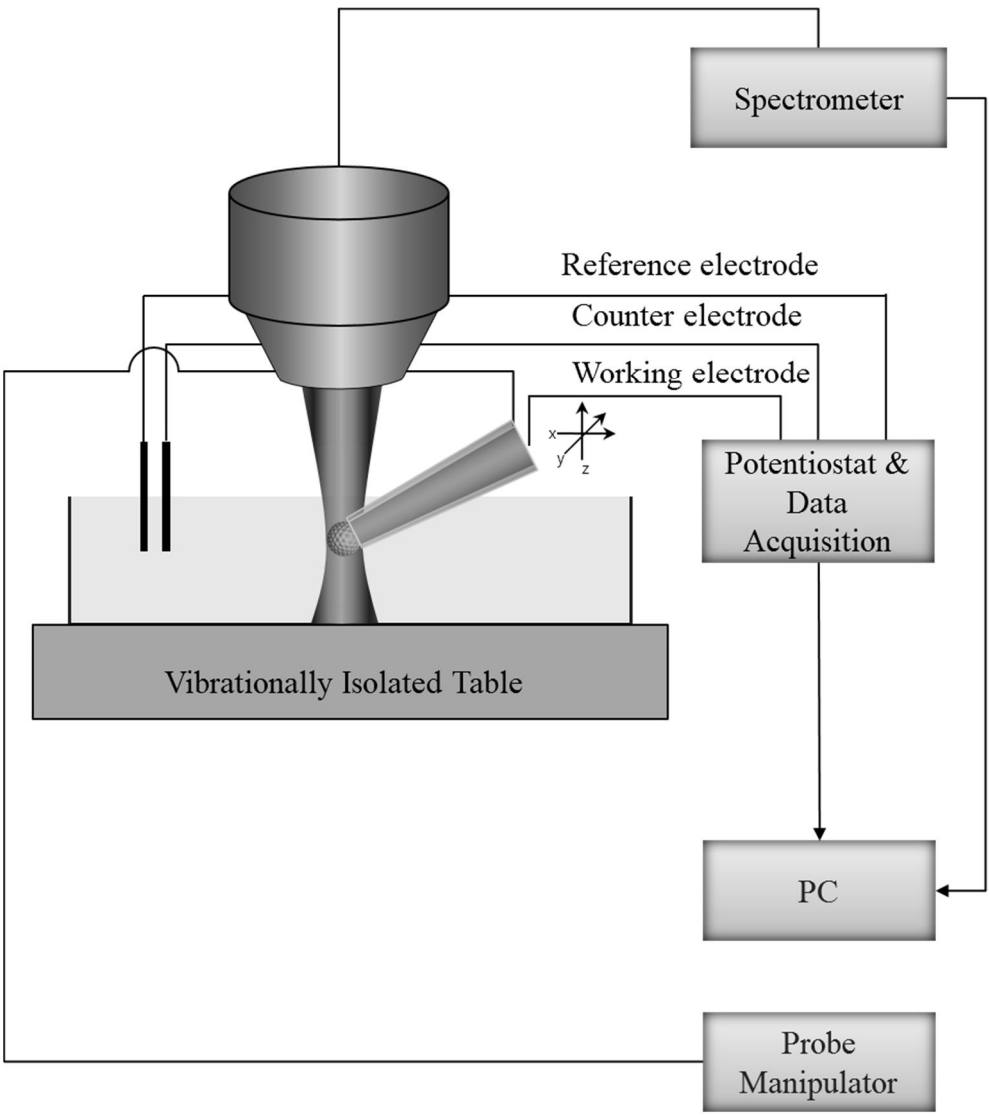


**Figure 3-6.** Schematic illustration of the proposed electrochemical SERS monitoring system based on a well-defined EC-SERS probe. A gold μ-shell *ca.* 2 μm in diameter at the end of the probe acts as a sensitive SERS substrate and a UME with well-defined geometry and dimensions. The μ-shell perfectly fits the focal volume of the laser beam used in this work, a He/Ne laser (632.8 nm, 3 mW).

Figure 3-6 showed a schematic view of the proposed system. We used a micromanipulator to position the probe as needed to collect EC-SERS signals from the molecules of interest in solution. The probe was tilted about 30 degrees to allow the laser beam to focus on the gold μ-shell and was connected with a potentiostat to acquire electrochemical data at the same time.

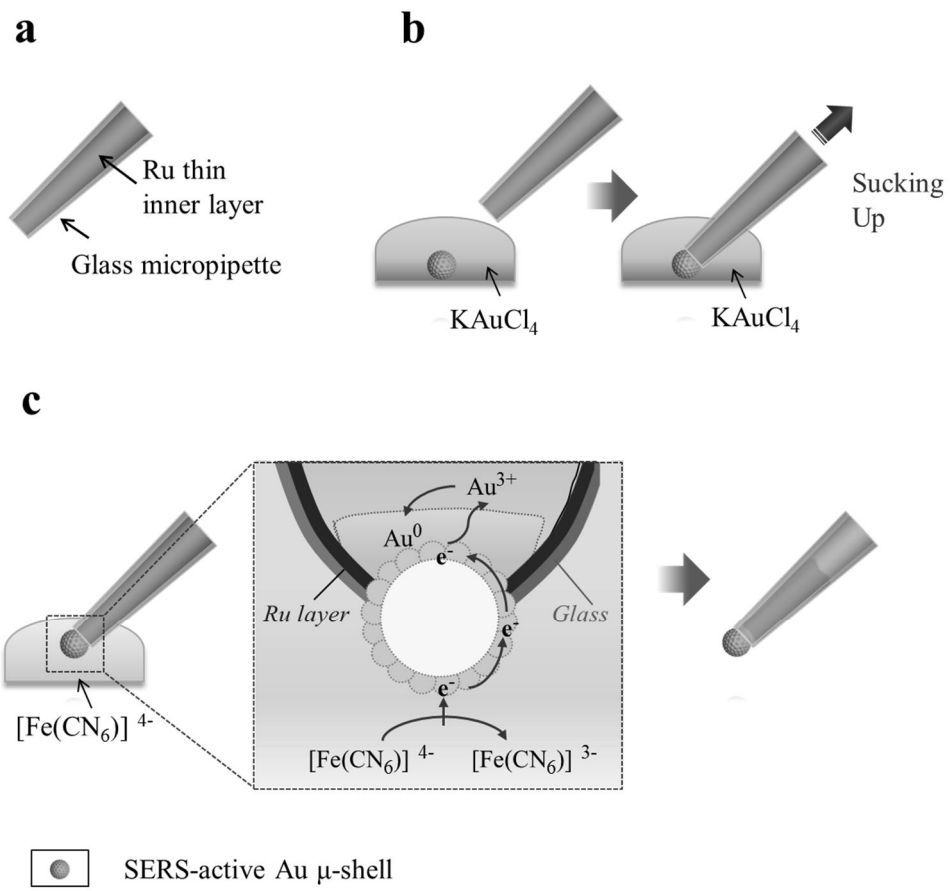

**Figure 3-7.** Fabrication of the EC-SERS probe. (a–b) A SERS-active gold μ-shell was simply attached to the end of a micropipette by suction with negative pressure, and (c) electrically connected with a conductive inner layer by heterogeneous electroless deposition.

Figure 3-7 showed the overall fabrication procedure for the EC-SERS probe. A glass micropipette was prepared by a conventional pulling method using a $CO_2$ laser puller. A ruthenium (Ru) thin film was deposited on the inside wall of the micropipette by atomic layer deposition (ALD)[29-30] to serve as an electrical contact (Figure 3-7(a)). ALD allowed successful deposition of a high-aspect-ratio structure on the micropipette without clogging, and the Ru thin film as made was superior in conductivity (with estimated resistivity of *ca.* 15 μΩ cm) to other materials such as the layers produced by graphitic carbonization in chemical vapor deposition.[31-32]

The gold μ-shells were optimized to release the strongest SERS under the conditions of given dimension and element which follow a previously reported process.[25] Gold nanoparticles (AuNPs) were adsorbed onto a polystyrene bead having amine terminals, and the AuNP-modified microspheres were exposed to a plating solution containing a mild reducing agent, formaldehyde, and a gold precursor, gold (III) chloride trihydrate. A microspherical gold shell expanded from the AuNP seeds to form over the surface.[25] The size of such gold μ-shells could be strictly controlled by carefully screening and selecting the polymer core, and the surface morphology could be controlled by employing an elaborate electroless

plating protocol. Consequently, we obtained gold μ-shells that have reproducible physicochemical properties.

Gold μ-shells as prepared were dispersed in a gold precursor solution containing 1 % potassium tetrachloroaurate (III). By applying negative pressure through the micropipette, we trapped one of the gold μ-shells at the end of the Ru-coated micropipette, which was filled with the same solution (Figure 3-7(b)). Then, the attached gold μ-shell was permanently fixed in mechanical and electrical contact with the inner Ru film by reducing the gold precursor on the inside surface of the μ-shell. The solution outside the micropipette was switched to a 0.25 M potassium ferrocyanide aqueous solution, which acted as a reducing agent to induce heterogeneous electron transfer to the gold precursor in the micropipette through the gold μ-shell (Figure 3-7(c)).

The Ru-coated micropipette ensured better electrical contact and insulation than previously reported UMEs employing electrophoretic paint[33] or carbonization.[31-32] Moreover, the assembly and fixing of bead based μ-shells and the Ru-coated micropipette preserved untainted active sites on the surface of the fixed μ-shell and greatly improve the sealing ability compared with conventional UMEs, in which a thin metal wire is buried in an insulating rod.[34-35] In addition, the shape of the probe electrode could be made nearly spherical or hemispherical by adjusting the relative sizes of the μ-shell and the micropipette end. The absolute size of the UMEs could be varied from sub-micrometer to a few tens of micrometers as well. Various types

of electrochemical measurement were possible with this system, allowing chemically and/or biologically modified UMEs.

## 3.2. Evaluation of the Functions of the EC-SERS probe

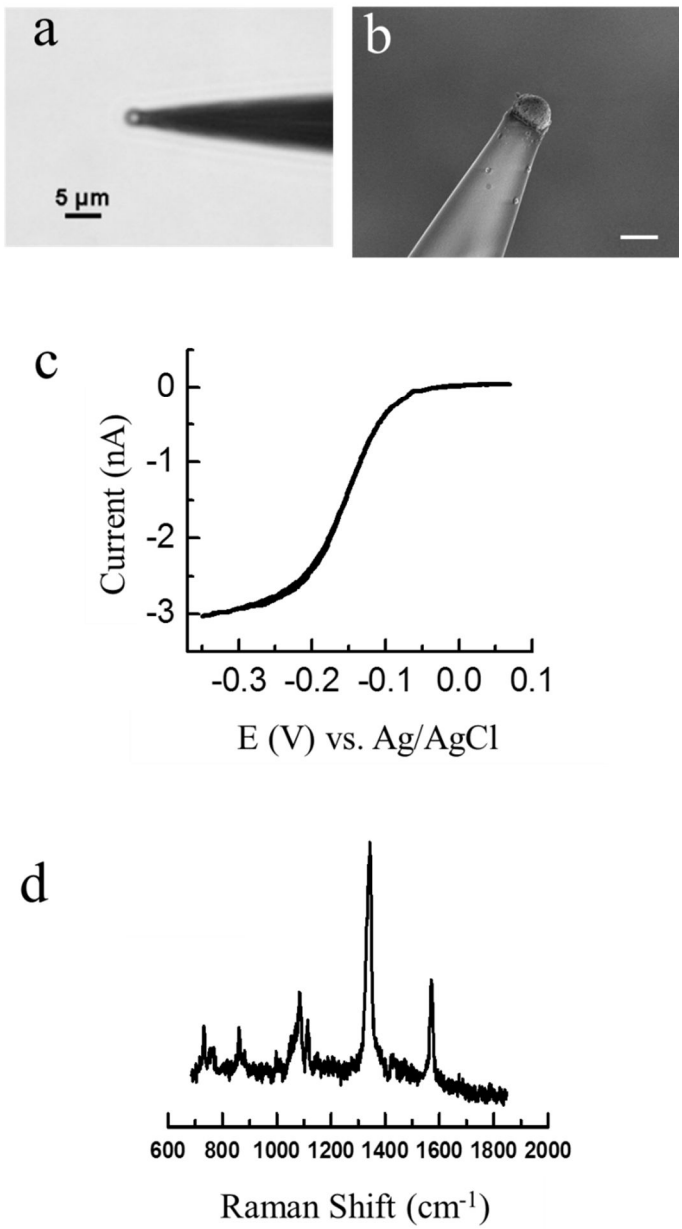


**Figure 3-8.** Construction and evaluation of the EC-SERS probe. (a) Optical and (b) FE-SEM image of the probe. Horizontal scale bar represents 2 µm. (c) Steady state voltammogram in 5 mM hexaammineruthenium (III) chloride aqueous solution

containing 0.1 M KCl as the supporting electrolyte (scan rate, 0.03 V $s^{-1}$). (d) SERS spectrum from the probe modified by 4-nitrobenzenethiol.

A FE-SEM image taken under very low electron beam power (2.0 kV) showed the glass micropipette to which a single gold μ-shell with a polymer core was attached (Figure 3-8(b)). It confirmed that the shape and size of the gold μ-shell were as expected in previous research.[25] Cyclic voltammogram of hexaammineruthenium (III) chloride (Figure 3-8(c)) revealed that the electrochemical behavior of this UME is the same as that of a typical UME used for SECM. The area of the electrochemically active surface, which was calculated from the diffusion-controlled steady state current, was comparable with the expected results which were devised from the FE-SEM image. We acquired the SERS spectra of 4-nitrobenzenethiol (NBT) adsorbed on the probe and assigned the peaks according to the literature (Figure 3-8(d)).[25]

## 3.3. *In situ* electrochemical SERS monitoring of NBT reduction and Py adsorbed on the EC-SERS probe

### 3.3.1. *In situ* electrochemical SERS monitoring of NBT reduction

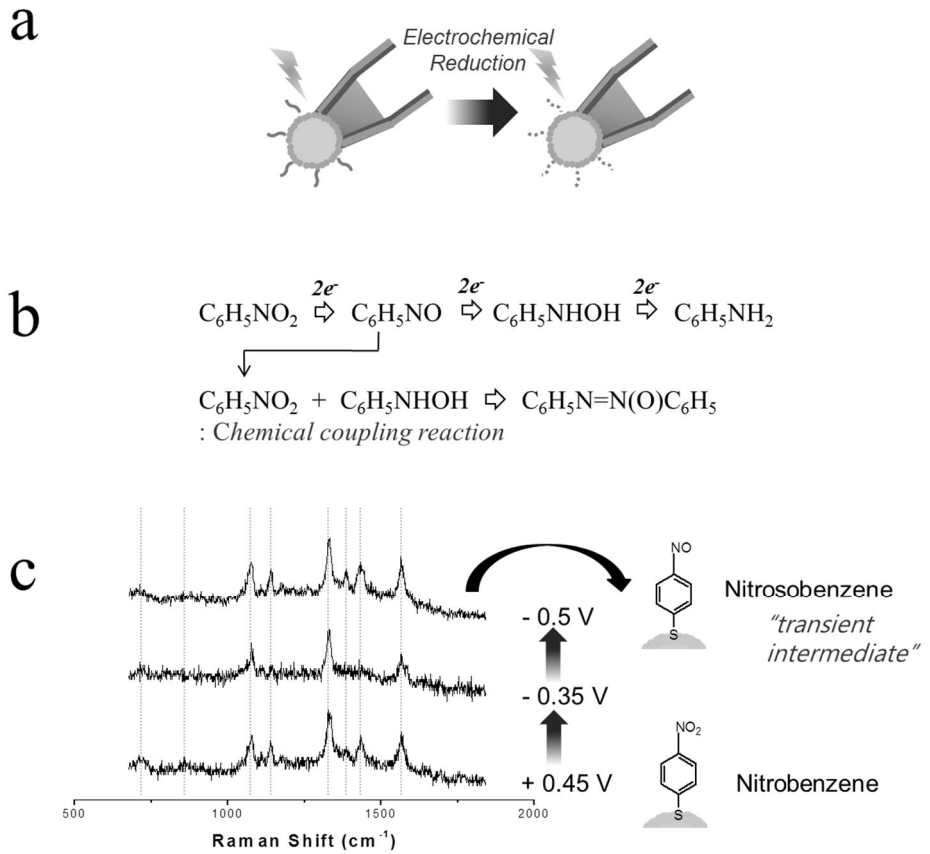


**Figure 3-9.** (a) The schematic view of the electrochemical reduction of the NBT on the probe, (b) a chemical equation of the reduction of nitrobenzene to aniline through three 2-electron steps, (c) potential dependent SERS spectrum in 0.1 M $H_2SO_4$.

To confirm the *in situ* performance of the EC-SERS tip, we monitored the electrochemical reduction of the NBT on the probe (Figure 3-9(a)). It is known that

nitrobenzene can be reduced to nitrosobenzene, phenylhydroxylamine, and aniline through three 2-electron steps (Figure 3-9(b)). Nitrosobenzene was difficult to detect because it may be consumed by chemical coupling reaction following the electrochemical reaction. Through the EC-SERS experiment, Nitrosobenzene molecules could be detected in 1988.[36] In Figure 3-9(c), we could detect nitrosobenzene at -0.5V and this result showed that our probe is useful tool to monitor a transient intermediate.

### 3.3.2. *In situ* electrochemical SERS monitoring of Py adsorbed

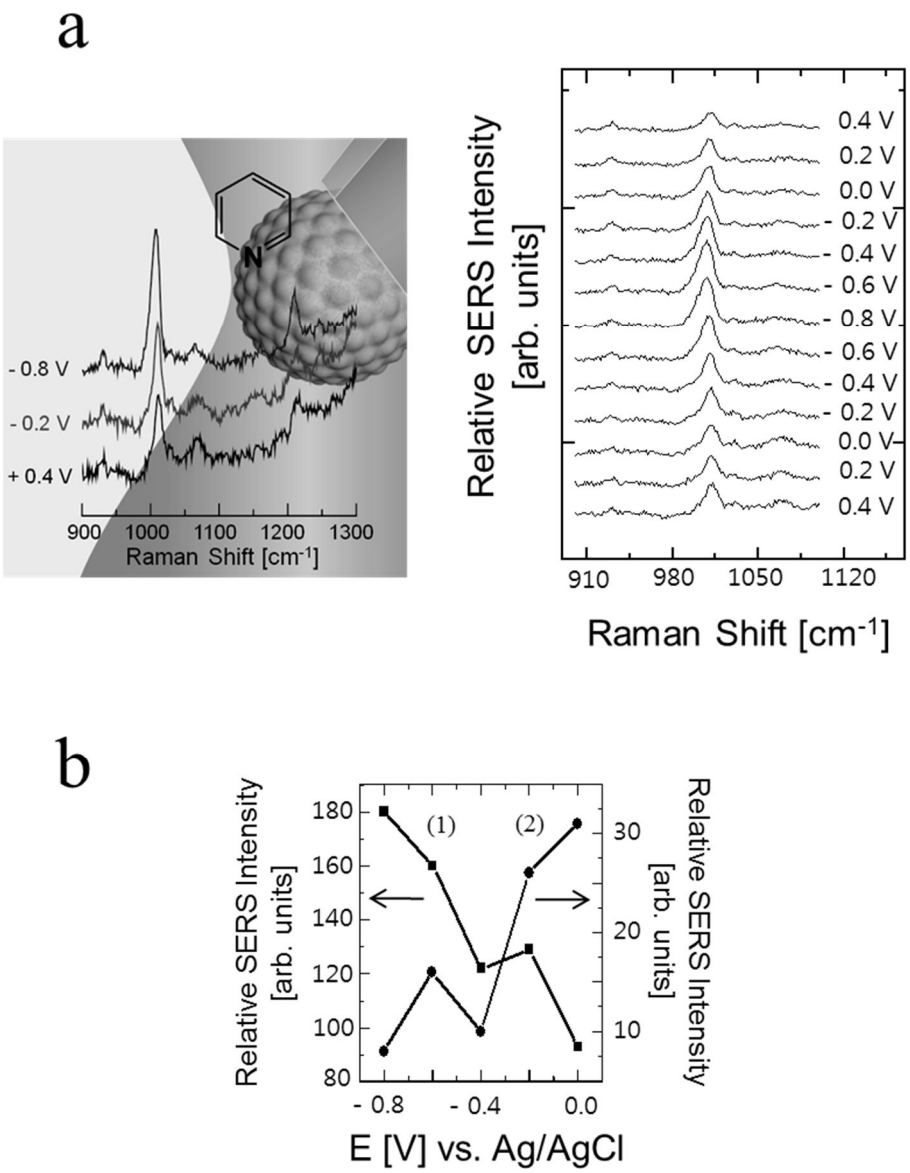


**Figure 3-10.** (a) SERS spectra of pyridine adsorbed on the gold μ-shell probe acquired at a variety of electrode potentials. Probe potential was swept from 0.4 V (bottom) to –0.8 V and back to 0.4 V (top) at 0.02 V $s^{-1}$. (b) Dependence of the

relative intensity of two bands, (1) *ca.* 1008 $cm^{-1}$ and (2) *ca.* 1029 $cm^{-1}$. The SERS intensity normalized by the aqueous perchlorate stretch band (*ca.* 930 $cm^{-1}$), which corresponds to the peak marked with an asterisk in Figure 3-4(a). All spectra were taken using a 632.8 nm line from a 3 mW He–Ne laser with an integration time of 10 s.

We also recorded potential–dependent vibrational spectra of adsorbed pyridine (Py), which was widely used to evaluate candidates for new EC-SERS substrate.[37-39] Figure 3-10 showed potential dependence of the characteristic peaks at *ca.* 1008 $cm^{-1}$, the ring breathing mode ($\nu_1$), and *ca.* 1029 $cm^{-1}$, C–H in-plane deformation ($\nu_{12}$), which were the evidences of the end-on configuration of the adsorbed Py molecules.[10,37] At more negative potential, the $\nu_1$ mode was enhanced in intensity and shifted from 1011 $cm^{-1}$ to 1008 $cm^{-1}$ (Figure 3-10(a) and (b-1)) while the $\nu_{12}$ mode was decreased in intensity (Figure 3-10(b-2)). These results were known for the changes in orientation of adsorbed Py molecules depending on electrochemical potential applied.[38-39] At more positive potential, $\pi$–type orbitals of the adsorbed Py molecules interacted with the metal surface to form flat configuration. As the potential applied became more negative, lone pair electrons of nitrogen form directly bond with the metal surface, resulting in upright or slightly tilted configurations.[10,38] In these regards, potential-dependent intensity of the $\nu_1$ and the $\nu_{12}$ modes in Figure 3-10(b) was consistent with the configuration properties that was previously mentioned. The $\nu_1$ vibrational stretch at more negative potential was

more likely to be hindered by the formation of thicker water layer at liquid-metal interfaces, thereby the corresponding peak undergoes red shift.[10,38] Peak intensity in the $\nu_1$ mode was recovered with only a little reduction when the electrode potential returned where it had been after a cyclic scan. (Figure 3-10(a)) This behavior showed that the probe provided a sufficiently stable platform for monitoring the SERS spectra as a function of electrochemical potential and could be reused for subsequent experiments without exchange. These observations concerning the frequency shift and intensity change of individual vibrational bands unequivocally told that the suggested EC-SERS probe produced *in situ* molecular information during interfacial electrochemical processes.

# 4. Conclusions

We propose a new EC-SERS probe prepared by assembling a SERS-active gold μ-shell and a micropipette with a highly conductive inner layer. This probe was characterized by cyclic voltammograms and SERS spectra of NBT adsorbed onto the electrode surface. Furthermore, we confirmed that the probe could simultaneously harvest *in situ* spectroscopic and electrochemical information at the same spot by acquiring SERS spectra of NBT and Py as a function of the applied potential. Since the presented probe is robust and allows precise control of its size and surface properties, it can act as a reliable electrode as well as a SERS substrate that can make highly sensitive and uniform enhancement in Raman signals across the substrate. In addition, versatile modification of the EC-SERS active gold μ-shells could offer specific functionalities such as selective detection or capture of molecular or larger targets. Accordingly, the proposed probe as a useful tool is expected to inspire unprecedented experimental approaches to fundamental chemical/electrochemical research including investigation of intermediate species involved in important reactions, monitoring of biochemical or chemical species that are released from the local domains of certain cell membrane, and many more applications.

# 5. References

(1) F.-R. F. Fan, J. Fernandez, B. Liu, J. Mauzeroll, in *Handbook of Electrochemisty*, Elsevier, Amsterdam, **2007**, pp. 471.

(2) A. Schulte, W. Schuhmann, *Angew. Chem.* **2007**, *119*, 8914-8933; *Angew. Chem., Int. Ed.* **2007**, *46*, 8760.

(3) S. Amemiya, A. J. Bard, F. R. F. Fan, M. V. Mirkin, P. R. Unwin, *Annu. Rev. Anal. Chem.* **2008**, *1*, 95.

(4) P. Bertoncello, *Energy Environ. Sci.* **2010**, *3*, 1620.

(5) K. L. Adams, M. Puchades, A. G. Ewing, *Annu. Rev. Anal. Chem.* **2008**, *1*, 329.

(6) C. Amatore, S. Arbault, M. Guille, F. Lemaitre, *Chem. Rev.* **2008**, *108*, 2585.

(7) D. L. Robinson, A. Hermans, A. T. Seipel, R. M. Wightman, *Chem. Rev.* **2008**, *108*, 2554.

(8) J. L. Fernandez, D. A. Walsh, A. J. Bard, *J. Am. Chem. Soc.* **2005**, *127*, 357.

(9) Fu-Ren F. Fan and Allen J. Bard, *Proc. Natl. Acad. Sci.* **1999**, *96*, 14222.

(10) M. Fleischm, P. J. Hendra, A. McQuilla, *Chem. Phys. Lett.* **1974**, *26*, 163.

(11) Z. Q. Tian, B. Ren, *Annu. Rev. Phys. Chem.* **2004**, *55*, 197.

(12) D. Y. Wu, J. F. Li, B. Ren, Z. Q. Tian, *Chem. Soc. Rev.* **2008**, *37*, 1025.

(13) L. Stolberg, J. Lipkowski, D. E. Irish, *J. Electroanal. Chem.* **1991**, *300*, 563.

(14) Z. Q. Tian, B. Ren, J. F. Li, Z. L. Yang, *Chem. Commun.* **2007**, 3514.

(15) R. M. Stockle, Y. D. Suh, V. Deckert, R. Zenobi, *Chem. Phys. Lett.* **2000**, *318*, 131.

(16) M. S. Anderson, *Appl. Phys. Lett.* **2000**, *76*, 3130.

(17) N. Hayazawa, Y. Inouye, Z. Sekkat, S. Kawata, *Opt. Commun.* **2000**, *183*, 333.

(18) B. Pettinger, G. Picardi, R. Schuster, G. Ertl, *Electrochemistry* **2000**, *68*, 942.

(19) B. Ren, G. Picardi, B. Pettinger, R. Schuster, G. Ertl, *Angew. Chem.* **2005**, *117*,141-144; *Angew. Chem., Int. Ed.* **2005**, *44*, 139.

(20) A. Rasmussen, V. Deckert, *J. Raman Spectrosc.* **2006**, *37*, 311.

(21) U. Neugebauer, P. Rosch, M. Schmitt, J. Popp, C. Julien, A. Rasmussen, C. Budich, V. Deckert, *ChemPhysChem* **2006**, *7*, 1428.

(22) D. H. Pan, N. Klymyshyn, D. H. Hu, H. P. Lu, *Appl. Phys. Lett.* **2006**, *88*.

(23) R. Singhal, Z. Orynbayeva, R. V. K. Sundaram, J. J. Niu, S. Bhattacharyya, E. A. Vitol, M. G. Schrlau, E. S. Papazoglou, G. Friedman, Y. Gogotsi, *Nat. Nanotechnol.* **2011**, *6*, 57.

(24) A. Weber-Bargioni, A. Schwartzberg, M. Cornaglia, A. Ismach, J. J. Urban, Y. J. Pang, R. Gordon, J. Bokor, M. B. Salmeron, D. F. Ogletree, P. Ashby, S. Cabrini, P. J. Schuck, *Nano Lett.* **2011**, *11*, 1201.

(25) L. Piao, S. Park, H. B. Lee, K. Kim, J. Kim, T. D. Chung, *Anal. Chem.* **2010**, *82*, 447.

(26) S. L. Westcott, S. J. Oldenburg, T. R. Lee, N. J. Halas, *Langmuir* **1998**, *14*, 5396.

(27) A. J. Bard, L. R. Faulkner, In *Electrochemical Methods - Fundamentals and Applications*; John Wiley & sons, Inc.: New York, 2001, p 171.

(28) M. Pyo, A. J. Bard, *Electrochim. Acta* **1997**, *42*, 3077.

(29) S. -H. Park, S. Kim, D.-J. Lee, S. Yun, Z. G. Khim, K.-B. Kim, *J. Electrochem. Soc.* **2009**, *156*, K181.

(30) D. J. Lee, S. S. Yim, K. S. Kim, S. H. Kim, K. B. Kim, *Electrochem. Solid State Lett.* **2008**, *11*, K61.

(31) B. M. Kim, T. Murray, H. H. Bau, *Nanotechnology* **2005**, *16*, 1317.

(32) M. G. Schrlau, E. M. Falls, B. L. Ziober, H. H. Bau, *Nanotechnology* **2008**, *19*.

(33) J. Abbou, C. Demaille, M. Druet, J. Moiroux, *Anal. Chem.* **2002**, *74*, 6355.

(34) B. Zhang, Y. H. Zhang, H. S. White, *Anal. Chem.* **2004**, *76*, 6229.

(35) C. G. Zoski, *Electroanalysis* **2002**, *14*, 1041.

(36) P. Gao et al. *J. Phys. Chem.* **1988**, 92, 7122

(37) T. H. Lin, N. C. Linn, L. Tarajano, B. Jiang, P. Jiang, *J. Phys. Chem. C* **2009**, *113*, 1367.

(38) M. E. Abdelsalam, P. N. Bartlett, J. J. Baumberg, S. Cintra, T. A. Kelf, A. E. Russell, *Electrochem. Commun.* **2005**, *7*, 740.

(39) W. H. Li, X. Y. Li, N. T. Yu, *Chem. Phys. Lett.* **1999**, *305*, 303.

# List of Publications

1. Donghoon Han, Sung Yul Lim, **Beom Jin Kim**, Lilin Piao, Taek Dong Chung*, "Mercury(II) detection by SERS based on a Single Gold Microshell", Chem. Commun. 46, 5587–5589 (2010)

2. Hyun Joo Jung, Inseong Hwang, **Beom Jin Kim**, Hyunung Yu, Hyegeun Min, Tae Geol Lee, Taek Dong Chung*, "Selective and Direct Immobilization of Cysteinyl Biomolecules by Electrochemical Cleavage of Azo Linkage", Langmuir 26(19), 15087-15091 (2010)

3. Ji-Hyung Han, Kwang Bok Kim, Je Hyun Bae, **Beom Jin Kim**, Chung Mu Kang, Hee Chan Kim, Taek Dong Chung*, "Ion Flow Crossing over a Polyelectrolyte Diode on Microfluidic Chip", Small 7(18), 2629-2639 (2011)

4. **Beom Jin Kim**, Do-Joong Lee, Yang-Rae Kim, Sung Yul Lim, Je Hyun Bae, Ki-Bum Kim, Taek Dong Chung*, "Gold Microshell Tip for in situ Electrochemical Raman Spectroscopy", Adv. Mater. 24, 421-424 (2012)

5. Solji Kim, Lilin Piao, Donghoon Han, **Beom Jin Kim**, Taek Dong Chung*, "Surface Enhanced Raman Scattering on Non-SERS Active Substrates and In Situ Electrochemical Study based on Single Gold Microshell", Adv. Mater. 25, 2056-2061(2013)

6. Je Hyun Bae, Chung Mu Kang, Hyoungseon Choi, **Beom Jin Kim**, Woohyuk Jang, Sung Yul Lim, Hee Chan Kim, Taek Dong Chung*, "Nonfaradaic Nanoporous Electrochemistry for Conductometry at High Electrolyte

Concentration", Anal. Chem. 87, 2443−2451 (2015)

7. **Beom Jin Kim**, Yang-Rae Kim, Minjee Seo, Eun Joong Kim, Joohee Jeon, Taek Dong Chung*, "Electrochemical Impedance Spectroscopy at Well Controlled dc Bias for Nanoporous Platinum Microelectrode in Embryo Brain", *submitted*

# 요약 (국문초록)

전기화학은 생체 분석과 표면 분석에 있어서 시료물질을 파괴하지 않고 그 자체를 연구할 수 있기 때문에 매우 효과적인 분석 방법이다. 이를 위해서 다양한 크기의 프로브가 사용되었고, 특히 마이크로 사이즈의 프로브는 적절한 해상도를 제공하기 때문에 실용적인 측면에서 매우 유용하다.

파트 1에서는 분석 방법에 대한 개관과 마이크로 사이즈 프로브의 필요성에 대해서 설명한다.

파트 2에서는 굉장히 작고 (1-2 nm) 균일한 구멍을 가진 나노포러스 백금인 $L_2$-ePt를 이용하여 쥐의 태아의 뇌에서 전기화학적인 분석을 수행하였다. 정확한 전기화학 전위를 조절하면서 나노포러스를 도금하기 전과 후를 비교하기 위해, 도금이 안된 평면 백금과 나노포러스 백금이 꼬여진 전극에 Ag/AgCl이 기준전극으로써 둘러 싸여 있는 전극을 태아의 뇌에 도입하여 전기화학 셀을 구축하였다. 평면 백금과 $L_2$-ePt는 뇌 안에서 각각 전압전류법과 전기화학적 임피던스 분석법으로 비교했고, 임피던스 분석에서 직류 전위는 전기화학 반응에 의한 간섭을 최소화하는 전위로 선택하였다. $L_2$-ePt의 전기화학적 거동을 확인한 결과, 뇌에서의 심각한 피막형성이 없으며, 평면 전극보다 이상적인 캐패시터에 가까움을 확인하였다. $L_2$-ePt의 낮은 전극 임피던스는 전극과 세포 외액 사이

의 계면에서의 전위 하강을 감소시켰고, 이는 시스템 전체를 심각한 부반응부터 보호하게 된다. $L_2$-ePt는 이렇듯 낮은 전극 임피던스와 전기화학적인 안정성을 가지고 있어 멀리 떨어진 세포에 자극을 가하는데 유리하고, 먼 곳에서 발생하는 local field potential과 같은 신호를 측정하는데 유용한 전극 재료로 기대된다.

파트 3에서는 전기화학 신호와 분광학적인 정보를 동시에 얻을 수 있는 새로운 전기화학 및 분광학 (EC-SERS) 프로브를 제안한다. EC-SERS 프로브는 표면산란 라만 분광법에 활성을 가진 금 마이크로 쉘과 이를 전도성을 가진 마이크로 피펫에 전기적으로 연결하는 과정을 통해 제작된다. 이때 이 두 성분은 특별한 무전해 도금 방법을 통해 결합 된다. EC-SERS 프로브는 레이저의 부피보다 작지만 현미경으로 보기에 적합한 2 μm사이즈이다. 이 프로브는 전기화학 및 생물학적인 시스템에 이전에 없던 많은 정보를 제공하는 효과적인 분석 도구가 될 것이라 기대된다.

주요어 : 나노포러스 전극, 신경측정과 자극, 마이크로프로브, 전기화학, 금 마이크로쉘, 라만 분광학, 초미세전극

학번 : 2007-22817